Tectonics

RESEARCH ARTICLE
10.1029/2022TC007677

**Key Points:**

- Thermochronology data support orogenesis in the southern Patagonian Andes (51°–53°S) from 50 to 35 Ma
- Results of our study require Eocene contractional deformation along the bend of the Patagonian orocline
- Exhumation driving the Paleogene foreland basin unconformity extended beyond the basin boundary

**Supporting Information:**

Supporting Information may be found in the online version of this article.

**Correspondence to:**

A. L. Stevens Goddard,
alsg@iu.edu

**Citation:**

Stevens Goddard, A. L., Fosdick, J. C., Calderón, M., Ghiglione, M. C., VanderLeest, R. A., & Romans, B. W. (2023). Thermochronological evidence for Eocene deformation in the southern Patagonian Andes: Linking orogenesis along the Patagonian orocline. *Tectonics*, *42*, e2022TC007677. https://doi.org/10.1029/2022TC007677

Received 11 NOV 2022
Accepted 13 MAR 2023

**Author Contributions:**

**Conceptualization:** A. L. Stevens Goddard, J. C. Fosdick, M. Calderón, M. C. Ghiglione
**Data curation:** A. L. Stevens Goddard, J. C. Fosdick, M. Calderón
**Formal analysis:** A. L. Stevens Goddard, M. C. Ghiglione
**Funding acquisition:** J. C. Fosdick, M. Calderón
**Investigation:** M. Calderón, M. C. Ghiglione
**Methodology:** A. L. Stevens Goddard, J. C. Fosdick
**Resources:** A. L. Stevens Goddard, J. C. Fosdick, M. Calderón
**Supervision:** A. L. Stevens Goddard, J. C. Fosdick
**Visualization:** A. L. Stevens Goddard, J. C. Fosdick, M. Calderón, M. C. Ghiglione, R. A. VanderLeest, B. W. Romans



# Thermochronological Evidence for Eocene Deformation in the Southern Patagonian Andes: Linking Orogenesis Along the Patagonian Orocline

**A. L. Stevens Goddard[1], J. C. Fosdick[2], M. Calderón[3], M. C. Ghiglione[4], R. A. VanderLeest[5], and B. W. Romans[6]**

[1]Department of Earth and Atmospheric Sciences, Indiana University, Bloomington, IN, USA, [2]Department of Earth Sciences, University of Connecticut, Storrs, CT, USA, [3]Carrera de Geología, Facultad de Ingeniería, Universidad del Desarrollo, Santiago, Chile, [4]Instituto de Estudios Andinos—CONICET, Universidad de Buenos Aires, Buenos Aires, Argentina, [5]Department of Life, Earth, and Environmental Sciences, West Texas A & M University, Canyon, TX, USA, [6]Department of Geosciences, Virginia Tech, Blacksburg, VA, USA

**Abstract** Thermochronologic results from zircon fission track and (U-Th)/He data collected across the Patagonian batholith, basement and thrust belt of the southern Patagonian Andes between 51°S and 53°S resolves new spatiotemporal patterns of Paleogene rock cooling that allows us to reconstruct deformational and erosional events along- and across-strike. Our study applies a novel modeling strategy, the Path Family Approach, to filter geologically plausible thermal solutions from inverse modeling results for rocks in this study according to a sample's structural and tectonic context. Our results identify minimal cooling and interpreted exhumation of batholith rocks throughout the Paleogene. However, in the western domain we identify synchronous cooling of Jurassic volcaniclastic rocks in the thrust belt both along- and across-strike between 50 and 35 Ma, which we interpret as a period of out-of-sequence deformation that coincides with the start of a distinct period of orogenesis in the Fuegian Andes (54°S). This finding may suggest that the southern Patagonian Andes and Fuegian Andes evolved as a connected orogenic system along the bend of the Patagonian orocline. In the central domain, modeled cooling of thermally reset Cretaceous basinal strata from 60 to 50 Ma corresponds to a well-recognized erosional unconformity in the adjacent Cenozoic foreland depocenter, indicating that contemporaneous exhumation occurred beyond the margins of the basin. Although not diagnostic, exhumation within the orogenic belt, beyond the Cenozoic foreland basin, provides a new regional context to interpret the cause of this regional erosion event. Collectively these results inform the Paleogene tectonic evolution of the orogen.

## 1. Introduction

The construction of Cordilleran orogenic systems along long-lived subduction zones occurs across discrete episodes of retroarc shortening, extension and neutral conditions (e.g., DeCelles et al., 2009; Horton, 2018). The organization of the lithosphere and upper crustal structures observed today reflect the cumulation of these constructive mountain building phases, intermediary periods between these episodes (neutral tectonic conditions), and modification by dynamic and isostatic forces found at plate boundaries (Dávila & Lithgow-Bertelloni, 2015; Dávila et al., 2010; Guillaume et al., 2013; Horton, 2018; Stevens Goddard & Fosdick, 2019). Recognizing the presence and timing of orogenic pulses among the aggregate history of mountain building is important for understanding how Cordilleran systems evolve in response to changing tectonic plate organization, subduction dynamics, and tectonic cyclicity (e.g., DeCelles et al., 2009; Horton, 2018; Jordan et al., 2001).

The southern Patagonian Andes constitutes an important orogenic belt along the South American margin, connecting the 7,000 km-long N-S trending Andean belt with the E-W trending Fuegian Andes along the Patagonian orocline (Figure 1). The geologic record along this subduction zone preserves evidence of an evolving and dynamic plate margin including several distinct periods of deformation and mountain building beginning in the early Late Cretaceous as well as foreland basin erosion in the Paleocene, and spreading ridge subduction in the Eocene. Deformation includes a Cenomanian–Campanian phase that marked the initiation and growth of a retroarc thrust belt system, followed by an Oligocene–Miocene phase of thrust belt advancement (P. Betka et al., 2015; Biddle et al., 1986; Winn & Dott, 1979; Fildani & Hessler, 2005; Fosdick et al., 2011, 2013; Ghiglione & Ramos, 2005; Ghiglione et al., 2019; Katz, 1963; Kraemer, 1998; Wilson, 1991). Between these episodes of

**Writing – original draft:** A. L. Stevens Goddard, J. C. Fosdick
**Writing – review & editing:** A. L. Stevens Goddard, J. C. Fosdick, M. Calderón, M. C. Ghiglione, R. A. VanderLeest, B. W. Romans

lithospheric shortening, from the Campanian through the early Oligocene, kinematic reconstructions suggest an intermediate period of deformation, but the timing, style, and continuity (e.g., continuous or episodic) of this deformational event have proved difficult to directly determine (P. Betka et al., 2015; Fosdick et al., 2011, 2020; Klepeis & Austin, 1997). A ∼10–15 Myr Paleogene regional unconformity in the retroarc foreland basin system (Biddle et al., 1986; Fosdick et al., 2015; George et al., 2020) preserves evidence of a significant erosional event and has led some workers to interpret a period of tectonic stasis during the Paleogene (George et al., 2020; Horton, 2018). The mechanism causing erosion associated with the Paleogene unconformity and the extent of erosion during this event beyond the foreland basin is unknown. In addition to structural reconstructions of contractional deformation, plate kinematic reconstructions indicate the subduction of the Farallon-Aluk spreading ridge in the early Eocene marking the initiation of Farallon plate subduction in the southern Patagonian Andes (Eagles & Scott, 2014; Somoza & Ghidella, 2012) which may have facilitated uplift (isostatic or geodynamic) of the South American Plate (Guillaume et al., 2010, 2013; Haschke et al., 2006; Ramos, 2005; Stevens Goddard & Fosdick, 2019).

Reconstructing the orogenic history of the southern Patagonian Andes during the latest Cretaceous–Paleogene has important implications for interpreting the effects of plate tectonic reorganizations on Cordilleran orogenesis. Key questions include: (a) Was there a period of Paleogene deformation in the southern Patagonian Andean thrust belt that corresponds with documented deformation in the Fuegian Andes? If so, this finding may suggest Eocene orogenesis in the southern Patagonian Andes is due to a major tectonic plate reorganization at ca. 50 Ma (Ghiglione et al., 2008; Lagabrielle et al., 2009; Scher & Martin, 2006; Somoza & Ghidella et al., 2012; van de Lagemaat et al., 2021). (b) Could erosion associated with a regional Paleogene unconformity in the retroarc foreland basin extend beyond the basin boundary and into the orogenic belt? Currently, there is no documented evidence of erosion during the Paleogene unconformity in the southern Patagonian Andes beyond the western edge of the foreland basin system; however evidence of concurrent exhumation in the batholith or thrust belt could help to determine the process responsible for this major regional erosion event (Fosdick et al., 2015; George et al., 2020; VanderLeest et al., 2022). (c) Is there evidence of Farallon-Aluk spreading ridge subduction along the western plate margin in the early to middle Eocene as proposed by tectonic plate reconstructions (Cande & Leslie, 1986; Eagles & Scott, 2014; Somoza & Ghidella, 2012)? Comparing the timing of ridge subduction from plate kinematic models with periods of deformation and exhumation/erosion is critical to understand the role of spreading ridge subduction on orogenesis (Iannelli et al., 2020; Navarrete et al., 2020; Ramos, 2005; Stevens Goddard & Fosdick, 2019; Thorkelson, 1996).

Resolving the latest Cretaceous—early Oligocene orogenic history of the southern Patagonian Andes has remained persistently challenging in part due to the missing rock record including the regional Paleogene unconformity in the foreland basin (Biddle et al., 1986; Fosdick et al., 2015, 2020; George et al., 2020; Ghiglione et al., 2016; Horton, 2022; Malumián et al., 2000; Sickmann et al., 2018) and magmatic hiatuses in the Paleogene which result in a paucity of datable geologic material (Hervé, Massonne, et al., 2007; Kay et al., 2004; Ramos, 1989). To overcome this issue, we use low-temperature thermochronology data and thermal history modeling to reconstruct the thermal record of rock heating and cooling across the southern Patagonian orogenic system between latitudes ∼51°S and 53°S (Figures 1 and 2).

## 2. Tectonic Context

### 2.1. Structural Domains

The orogenic system of the southern Patagonian Andes between 51°S and 54°S can be divided into four major tectonomorphic domains (Figure 1) with distinct lithologies and deformational histories that chronicle Mesozoic–Cenozoic plate-margin processes across extensional and compressional orogenic cycles (Fosdick et al., 2013; Muller et al., 2021). From west to east, these domains include the accretionary complexes, and the western, central, and eastern thrust belt domains (Figure 1; Ghiglione et al., 2009; Fosdick et al., 2013; Muller et al., 2021).

The accretionary complex domain, west of the domains sampled in this study, includes the Madre de Dios and Diego de Almagro accretionary complexes that were frontally and basally accreted to the continental margin, respectively, throughout the Mesozoic times (Angiboust et al., 2018; Hyppolito et al., 2016; Willner et al., 2004, 2009). The juxtaposition of blueschist and amphibolite facies rocks with low grade metasedimentary rocks within the Cretaceous accretionary wedge occurred during the earliest Paleogene signaling a phase of shortening along the continental margin (Willner et al., 2004).

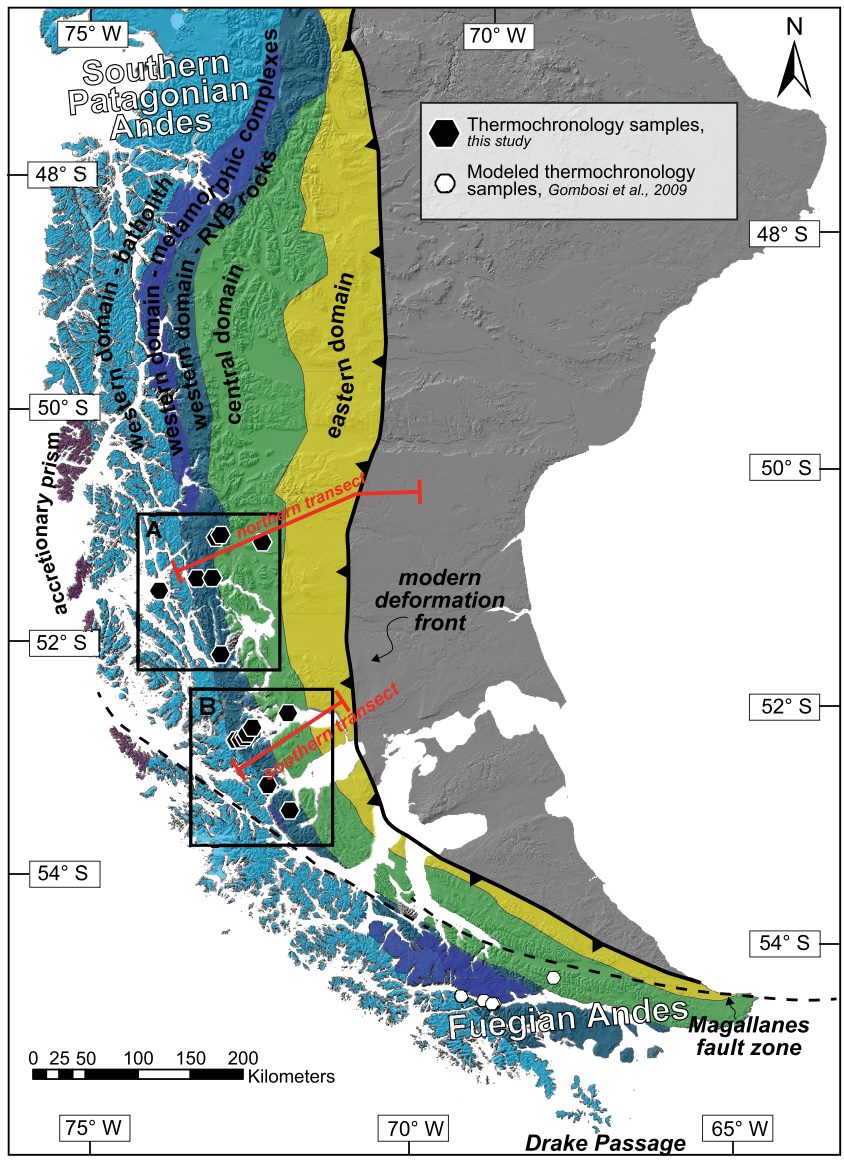


**Figure 1.** Summary location diagram identifying the tectonomorphic domains in the southern Patagonian and Fuegian Andes (P. Betka et al., 2022; Fosdick et al., 2013; Ghiglione et al., 2009; Muller et al., 2021; Thomson et al., 2001). The western domain is divided into three subdomains to identify batholith rocks, metamorphic core complexes, and the volcaniclastic and clastic rocks of the Rocas Verdes Basin (RVB). The location of the modern deformation front and Magallanes fault zone follows interpretations from Ramos (1989), Klepeis (1994), and Fosdick et al. (2011). The location of thermochronology samples analyzed and modeled in this study are indicated by black dots. The location of previously modeled multi-method thermochronology data sets from Gombosi et al. (2009) are indicated by white dots. Black boxes show the location of inset regional maps in Figure 2 (Box A) and 2B (Box B). Red lines indicate the location of cross sections through the northern and southern transects in Figure 3.

The western domain can be divided into (a) the plutonic rocks of the Patagonian batholith, (b) Mesozoic metamorphic morphic core complexes and (c) the metavolcaniclastic and hypabyssal rocks associated with the Rocas Verdes Basin (RVB) (Figure 1) that each have unique deformational and exhumational histories (Calderón et al., 2012, 2016; Fosdick et al., 2011, 2013; Ghiglione et al., 2009; Hervé, Massonne, et al., 2007; Thomson et al., 2001). The batholith rocks of the western thrust belt domain include the Jurassic–Neogene calc-alkaline plutons of the Patagonian batholith (Figures 1 and 2; Fanning et al., 2011; Hervé, Massonne, et al., 2007; Torres García et al., 2020). Batholith rocks are tectonically juxtaposed with Cretaceous metamorphic assemblages associated with long-lived subduction along the South American continental margin (Hervé, Massonne, et al., 2007;

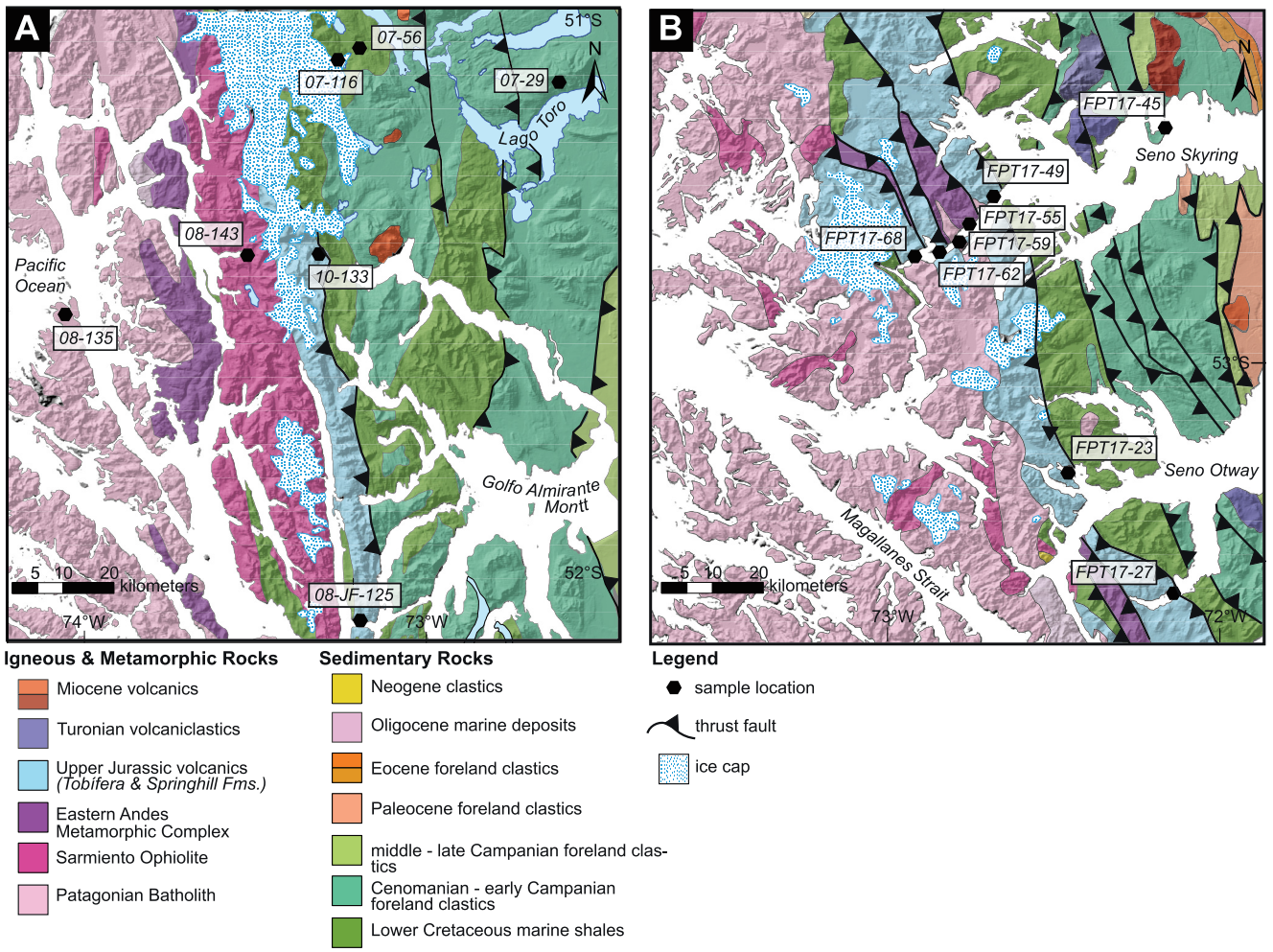


**Figure 2.** Local geologic maps adapted from SERNAGEOMIN (2003), Fosdick et al. (2013), and P. M. Betka (2013). Regional context is identified by the insets in Figure 1. Thermochronology sample locations in the northern transect (2A) and southern transect (2B) are shown with black circles and labeled.

Hervé, Pankhurst et al., 2007). Backarc extension in the Late Jurassic–Early Cretaceous rifted batholith rocks from the continental margin creating an oceanic-type marginal basin, the RVB, which opened northward to as far north as present-day 49°S (Dalziel et al., 1974; Malkowski et al., 2016; Stern & de Wit, 2004). Closure of the RVB commenced in middle Cretaceous time and culminated in an arc-continent collision which triggered development of the Late Cretaceous thrust belt along the Patagonian Andes (P. Betka et al., 2015; Calderón et al., 2012, 2016; Dalziel et al., 1974; Fildani & Hessler, 2005; Klepeis et al., 2010; Wilson, 1991); however, previous work suggests that batholith rocks have not been exhumed from depths ≥8 km by deformational processes after basin closure (Thomson et al., 2001). Arc magmatism and retroarc lithospheric shortening continued episodically during Cenozoic time (Fosdick et al., 2011; Hervé, Massonne, et al., 2007; Ramírez de Arellano et al., 2021; VanderLeest et al., 2020).

The metavolcaniclastic rocks of the western thrust belt domain (Figure 1; Ghiglione et al., 2009, 2014) constitutes antiformal duplex structures and high-angle thrust blocks that deform crustal remnants of the extensional RVB. These units include Paleozoic metamorphic rocks and the magmatic rocks of the Sarmiento Ophiolitic Complex and contemporaneous silicic volcaniclastic and hypabyssal intrusions of the Tobífera/Springhill Formation emplaced between ca. 160 and 140 Ma (Figure 2; Calderón et al., 2007; Hervé, Massonne, et al., 2007; Malkowski et al., 2016; Muller et al., 2021; Pankhurst et al., 2000). The distinct magmatic history and structural position of the Tobífera/Springhill Formation within thrust sheets of the western thrust belt domain make it an ideal target for thermochronological sampling (Figure 2). Overlying these successions are the marine shales of the Zapata/Erezcano Formation deposited during the post-rift sag phase of basin development that continued until ca. 100 Ma (Calderón et al., 2007;

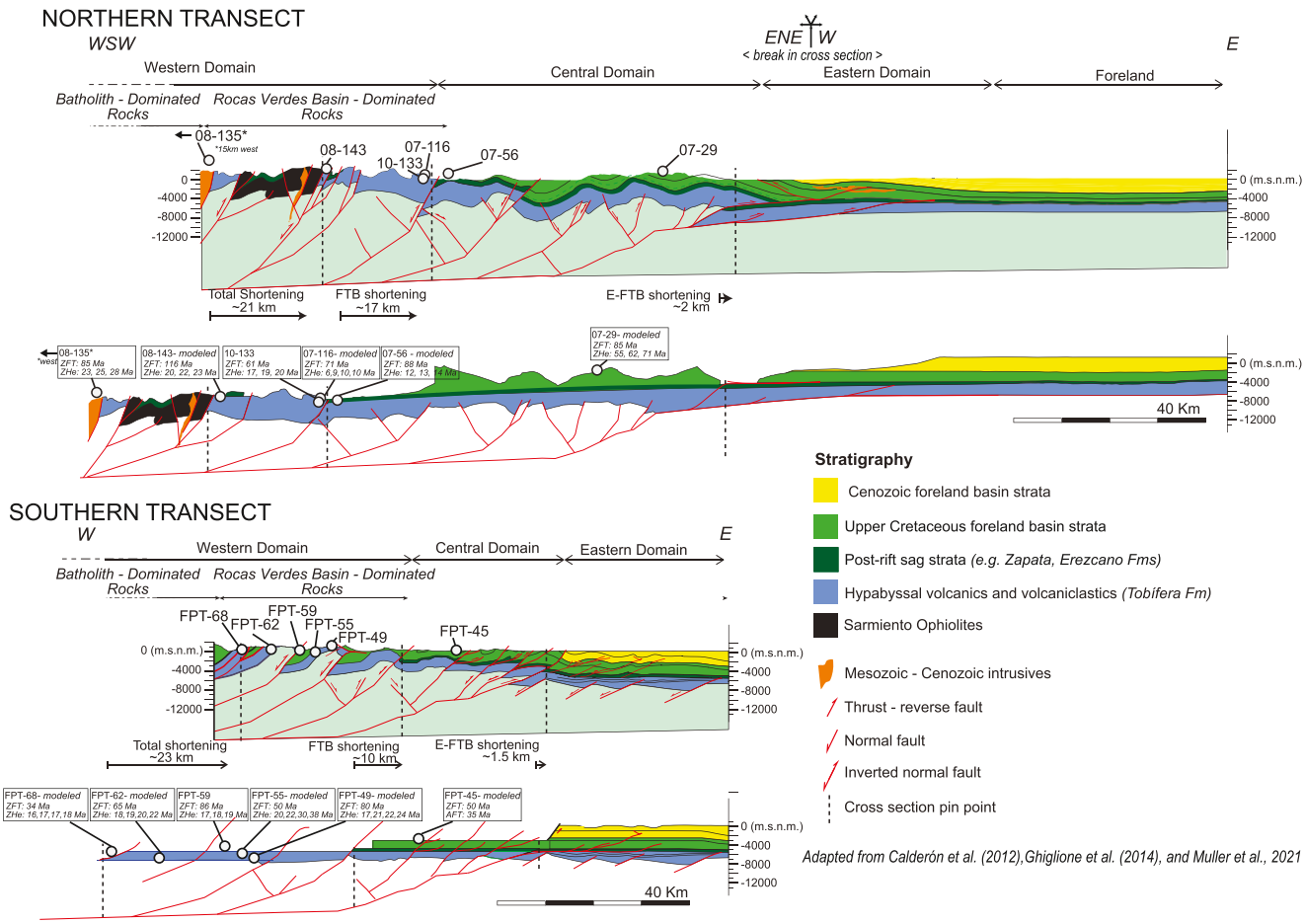


**Figure 3.** Structural cross sections and reconstructions adapted from Calderón et al. (2012), Ghiglione et al. (2014, 2019), and Muller et al. (2021) with locations of thermochronology samples on deformed and restored cross sections. Restored cross sections indicate ZFT, ZHe, and AFT cooling ages (errors can be found in data tables). Location of cross sections can be found in Figure 1.

Fildani & Hessler, 2005; Fosdick et al., 2011). The closure of the RVB and the initiation of contractional deformation within the Andean retroarc region incorporated these rocks into duplex structures and doubly vergent basement thrust blocks (Calderón et al., 2012; Fildani & Hessler, 2005; Fosdick et al., 2011; Wilson, 1991). Eastward vergent structures associated with intermediate-pressure, low-temperature greenschist-grade metamorphic conditions (Hervé, Pankhurst, et al., 2007; Muller et al., 2021) provide evidence of westward subduction and underthrusting of RVB rocks under continental arc fragments during basin closure (P. Betka et al., 2022; Calderón et al., 2012, 2016; Klepeis et al., 2010; Muller et al., 2021). Lithospheric thickening and topographic growth during this phase of orogenesis generated a thick succession of retroarc foreland basin deposits in a deep marine flexural foredeep of the Magallanes-Austral Basin (Biddle et al., 1986; Fildani & Hessler, 2005; Romans et al., 2010; Wilson, 1991).

The central thrust belt domain (Figures 1 and 3) is characterized by tight to open folding and thick-skinned faulting within the Jurassic Tobífera Formation, Lower Cretaceous Zapata/Erzecano formations, and Upper Cretaceous clastic foreland basin strata (e.g., Punta Barrosa and Cerro Toro Formations) of the Magallanes-Austral Basin (Figure 2; P. Betka et al., 2015; Fosdick et al., 2011; Ghiglione et al., 2009; Wilson, 1991). The underlying Tobífera Formation across this domain is deformed by thrust faults (Figures 2 and 3). Most of the exposed rocks in the central thrust belt domain constitute the ca. 92–65 Ma synorogenic deep-water foreland basin strata (Daniels et al., 2019; Romans et al., 2010; Wilson, 1991) including the conglomeratic members of the Upper Cretaceous submarine channel belt deposits (e.g., Cerro Toro and Escarpada Formations sampled in this study; Bernhardt et al., 2012; Daniels et al., 2019; Hubbard et al., 2008; Jobe et al., 2010; McAtamney et al., 2011).

The eastern thrust belt domain (Figure 1) is characterized by thin-skinned style thrust sheets that deform the latest Cretaceous through Cenozoic foreland basin strata culminating in an east-dipping frontal monocline

(Figure 2; P. Betka et al., 2015; Fosdick et al., 2011, 2013; Ghiglione et al., 2009, 2014). The southern Patagonian foreland basin strata within this domain preserve a ca. 15–20 My regional Paleogene unconformity between upper Cretaceous/lower Paleocene rocks and overlying Eocene units that has been interpreted to represent the erosion of 2–5 km of lower Paleocene strata (Biddle et al., 1986; Fosdick et al., 2011, 2015; George et al., 2020; Sickmann et al., 2018). This unconformity is well documented in contemporaneous foreland strata along strike of the orogenic system, but it is not clear if this erosional event also removed material from the western and central thrust belt domains. Although this study does not sample rocks from the eastern thrust belt, the timing and style of deformation and erosion in this domain provide regional context for interrogating linked thermal histories of rocks in the three westward domains.

### 2.2. Timing of Retroarc Deformation

The timing and sequence of thrusting during Cretaceous–Paleogene deformation in the southern Patagonian Andes bears directly on long-term record of rock exhumation (Figures 1 and 3). Geochronologic, geobarometric, and structural data from the basement thrust belt indicate that obduction of the Sarmiento Ophiolitic Complex and incipient structural growth of the thrust belt occurred between ca. 100 and 88 Ma via deformation along basement reverse structures such as the Canal de Las Montañas/Eastern Tobífera Shear Zone (e.g., Calderón et al., 2012; Muller et al., 2021). Subsequent development of the eastward verging thrust faults with basal detachments beneath the Tobífera and Zapata Formations created a series of stacked thrust sheets in the metavolcanic rocks of the western thrust belt domain between ca. 88 and 74 Ma (Albano Garcia et al., 2023; P. Betka et al., 2015, 2022; Fosdick et al., 2011; Ghiglione et al., 2019; Klepeis et al., 2010; Figure 3). Post emplacement or depositional burial of rocks from the Tobífera and Zapata Formations was facilitated by pre-deformational burial under the clastic rocks of the Zapata Formation, incorporation into the subduction channel during closure of the RVB, and by burial under imbricate thrust sheets.

The metamorphic P-T conditions and existing thermochronology data exhibit a wide range of burial conditions depending on the geographic and structural position of the samples. Rocks from the Tobífera Formation nearest the Canal de las Montañas shear zone exhibit evidence of low temperature metamorphism with sustained burial to depths >5 km and up to 15 km until at least ca. 80 Ma (Calderón et al., 2012; Muller et al., 2021). Burial estimates of rocks from the Tobífera and Zapata Formations lacking metamorphic textures can be inferred from thermochronometric systems reset after shallow emplacement or deposition. Previous thermochronology work in the Ultima Esperanza District (~51°S–51.5°S) indicates that the ZHe system, with an effective closure temperature of between 140 and 220°C, was fully reset for nearly all rocks from the Tobífera Formation in the western thrust belt domain (Fosdick et al., 2013). K-Ar analysis of authigenic illite targeting Tobífera and Zapata samples from deep structural levels in the western thrust belt domain shows evidence of exposure to temperatures of ~320 ± 20°C between the Cenomanian and early Eocene (Süssenberger et al., 2018). Assuming surface temperatures of 10°C and a geothermal gradient of 30 ± 5°C, this suggests unmetamorphosed samples were buried to at least ~6 km and to depths as great as ~10 km. In the southernmost Patagonian Andes, south of ~53°S, and in the eastern Fuegian Andes, late Paleocene to Middle Eocene exhumation has been interpreted to record deformation in the hanging wall of thrust faults in the western thrust belt domain (Barbeau et al., 2009; P. Betka et al., 2015; Ghiglione et al., 2014; Gombosi et al., 2009; Klepeis et al., 2010; Kohn et al., 1995).

The location of the faults and folds in the western and central thrust belt domains are defined by field-data and limited 2D seismic-reflection sections (Gallardo Jara et al., 2022) used to construct balanced cross sections modified from published work (Albano Garcia et al., 2023; P. Betka et al., 2015; Fosdick et al., 2011, 2013; Ghiglione & Ramos, 2005; Ghiglione et al., 2014; Klepeis & Austin, 1997; Klepeis et al., 2010), as summarized in Figure 3. In the Ultima Esperanza District (~51°S–51.5°S) thin-skinned propagation of the fold thrust belt into the strata of the Rocas Verdes and Magallanes basins is broadly constrained between the latest Cretaceous and Oligocene times. K-Ar cooling ages from individual thrust sheets suggest an Eocene phase of out-of-sequence deformation in the central thrust belt domain (Süssenberger et al., 2018), a timing consistent with regional provenance changes in the contemporaneous foreland basin attributed to thrusting (Fosdick et al., 2020). Fewer chronometric constraints exist in our study area south of Seno Otway at ~53°S, where fault kinematic analyses show that the Neogene Magallanes-Fagnano strike-slip fault system reactivates Cretaceous-Paleogene contractional structures (P. Betka et al., 2016; Klepeis et al., 2010).

Resolving the Paleogene history of exhumation and erosion within the tectonomorphic domains of the southern Patagonian orogenic system is essential to evaluating the geologic record of tectonic plate reorganization. A period of thrust fault deformation (Río Bueno thrusting) and rock exhumation in the Fuegian Andes observed

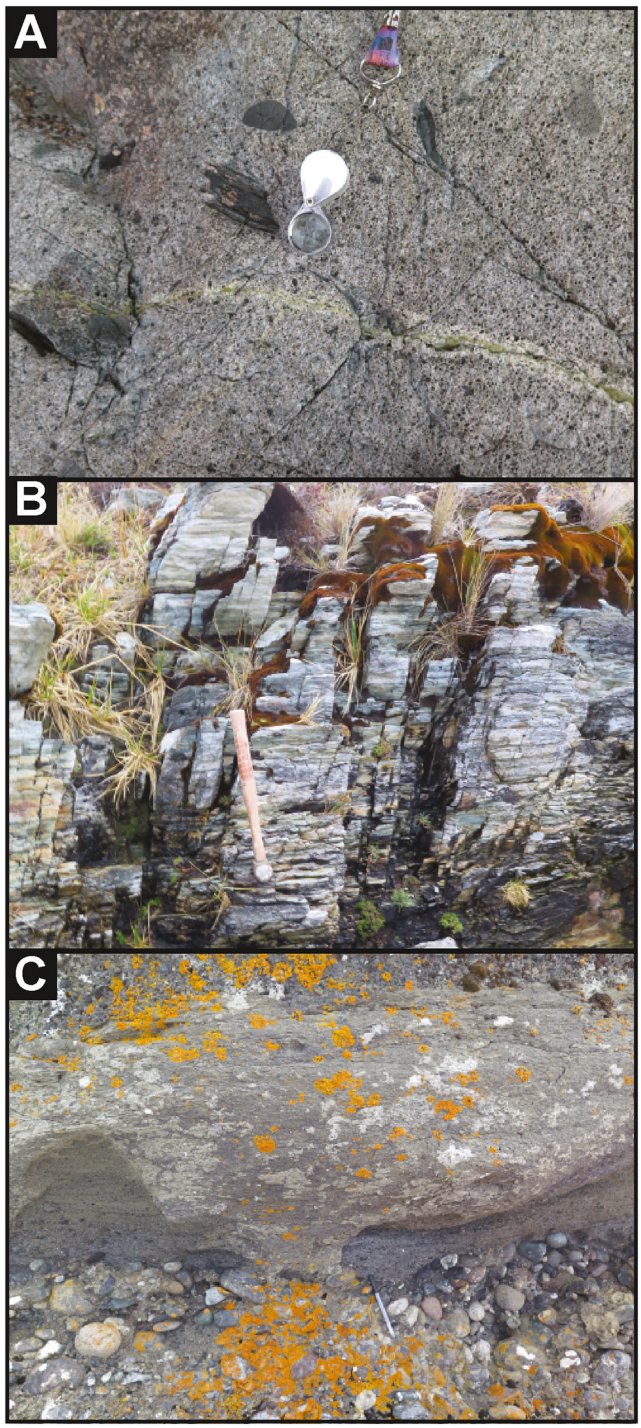


**Figure 4.** Representative outcrop photos of lithologies sampled for low temperature thermochronology. (a) Diorite intrusion in the batholith rocks of the western thrust belt domain. (b) Metarhyolite of the Tobífera Formation located in the western thrust belt domain. (c) Upper Cretaceous foreland basin strata including a conglomerate lens (typical of those sampled in this study) exposed in the central thrust belt domain.

at ca. 50 Ma is attributed to plate reorganization that occurred during an early stage in the opening of the Drake Passage which preceded the ca. 30 Ma onset of sea floor spreading in the Scotia Sea and ensuing strike-slip deformation along the Magallanes-Fagnano (Ghiglione & Ramos, 2005; Ghiglione et al., 2008; Gombosi et al., 2009; Kohn et al., 1995). This early event may have also triggered deformation in the southern Patagonian Andes (Fosdick et al., 2020). Spreading ridge subduction and slab window formation in the early to middle Eocene may also have modified regional geodynamics (Cande & Leslie, 1986; Eagles & Scott, 2014; Ramos, 2005; Somoza & Ghidella, 2012) as ridge subduction is shown to have isostatic and dynamic effects on the overriding plate that may contribute to exhumation and erosion across tectonomorphic domains (Guillaume et al., 2009, 2010; Stevens Goddard & Fosdick, 2019).

## 3. Low-Temperature Thermochronology Methods

Low temperature thermochronology captures the thermal history of rocks in response to geologic processes that drive rock cooling (including tectonic and erosional exhumation, and a cooling geothermal gradient) and heating (including thrust and sediment burial, contact heating, and a warming geothermal gradient). Previous work in the southern Patagonian Andes demonstrates that thermochronometers sensitive to temperatures below 120°C primarily preserve Neogene thermal signals (Christeleit et al., 2017; Fosdick et al., 2013; Herman & Brandon, 2015; Herman et al., 2013; Stevens Goddard & Fosdick, 2019; Thomson et al., 2001, 2010; Willett et al., 2020). Consequently, we apply the zircon fission track (ZFT) and zircon (U-Th)/He (ZHe) thermochronology systems with bulk closure temperatures of ~185–285°C and ~140–220°C, respectively, (Bernet, 2009; Guenthner et al., 2013; Ketcham, 2019; Reiners et al., 2004; Zaun & Wagner, 1985) to better constrain older (pre-Neogene) cooling.

Samples were collected for ZFT and ZHe thermochronology from two orogen-perpendicular transects including a northern transect at ~51°–51.5°S and a southern transect at ~52.5–53°S (Figures 1–3). Sampled lithologies include granodiorite, diorite, and metarhyolite from the Patagonian batholith in the western thrust belt domain ($n$ = 3), metarhyolite, rhyolite, and silicic volcaniclastic rocks from the Jurassic Tobífera Formation in the western thrust belt domain ($n$ = 10), and granitic conglomerate clasts from the Upper Cretaceous Cerro Toro and Escarpada Formations in the central thrust belt domain ($n$ = 2) (Figure 4). Standard 3–5 kg samples were collected (except for clasts). For conglomerate clasts, a single cobble-sized clast was selected per location and all minerals were extracted and analyzed from the same clast sample. Zircons were extracted using standard, crushing, sieving, magnetic, and density separation techniques. Separates were used to produce 14 new ZFT ages. ZHe ages from four samples are reported for the first time in this study along with ZHe ages from nine samples from previous work by Fosdick et al. (2013) and Stevens Goddard and Fosdick (2019) that come from the same samples as new ZFT ages. For one sample lacking ZHe data, we incorporate apatite fission track data from Stevens Goddard and Fosdick (2019).

### 3.1. Zircon (U-Th)/He (ZHe)

Zircon (U-Th)/He thermochronology measures production and retention of $^{4}$He in an individual zircon crystal produced by the decay of $^{238}$U, $^{235}$U, $^{232}$Th. At high temperatures, $^{4}$He naturally diffuses through the

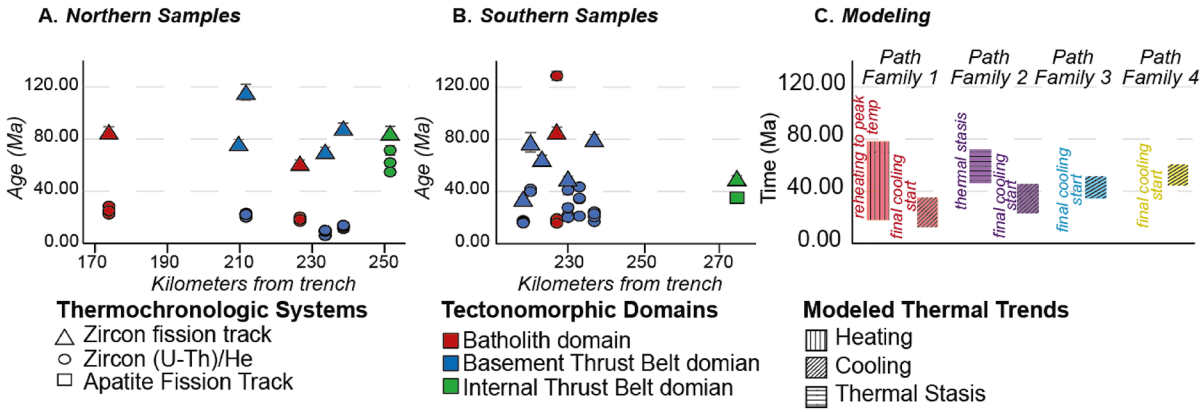


**Figure 5.** Diagrams summarizing thermochronology results from this study including cooling ages (a), (b), and modeling results (c). Importantly, cooling ages alone do not always correlate with a heating or cooling trend in the modeling results. (a), (b) Cooling ages from new and published thermochronology data sets used to constrain thermal history models from the northern transect (a) and southern transect (b) in this study. (c) Summary of major periods of heating, cooling, and stasis for the unique Path Families identified by inverse modeling of multi-method, multi-chronometer data sets.

crystal lattice and is lost from the mineral system; however, at low temperatures, $^{4}$He is retained in the zircon. Partial retention of $^{4}$He can occur between temperatures of 50 and 200°C depending on the crystal size and accumulated radiation damage; however partial $^{4}$He retention most commonly occurs between temperatures of 170 and 200°C (Guenthner et al., 2013). Zircon were selected for (U-Th)/He analysis according to clarity, size and shape (whole grains) using a Leica M 165 binocular microscope at the University of Connecticut. Single grain aliquots were packed and sealed in crimped Nb tubes. For ZHe analyses we analyzed four single grain aliquots per sample.

Laser heating gas extraction and chemical dilution were conducted at the University of Colorado Boulder Thermochronology Research and Instrumentation Lab. Nb-packed aliquots were loaded in an ASI Alphacron to extract and measure He gas. A 25W diode laser heated the aliquot to ca. 800–110°C for 5–10 min to extract $^{4}$He gas. A spike of 13 ncc $^{3}$He was used to spike extracted $^{4}$He gas and analyzed on a Balzers PrismaPlus QME 220 quadrupole mass spectrometer. Fish Canyon zircon standards were analyzed intermittently with unknown samples. Zircon grains and niobium tubes are dissolved in a series of HF solutions—the first spiked with a $^{235}$U, $^{230}$Th, $^{145}$Nd tracer—and a final $HNO_3$:HF mixture Sample solutions are analyzed for U, Th, and Sm on a Thermo Element 2 magnetic sector ICP-MS. ZHe dates were calculated using U, Th, and Sm measurements and grain geometries were used to correct for alpha ejection for single grain aliquots.

### 3.2. Zircon Fission Track (ZFT)

The decay by fission of $^{238}$U in zircon produces a physical zone of damage, called a fission track, in the host mineral that when etched by acid is optically identifiable. At temperatures below the closure temperature of the system, tracks are fully preserved, whereas at temperatures above the closure temperature of the system, tracks are annealed. The partial annealing zone (PAZ) marks the temperature transition between track preservation and annealing. Studies suggest a PAZ between ~185 and 280°C (Bernet, 2009; Ketcham, 2019; Zaun & Wagner, 1985). ZFT ages were generated using the external detector method at the University of Arizona Fission Track Lab. Zircon grains were mounted in teflon, polished to expose the grain, and etched in a eutectic solution of KOH and NaOH until tracks were optically identifiable (Garver, 2003). Mica sheets were affixed to the grain mounts of zircon, and samples were irradiated at Oregon State University. Mica prints were etched in 49% hydrofluoric acid for 45 min at 23°C to expose induced tracks.

## 4. Low-Temperature Thermochronology Results

Fourteen new ZFT ages generated in this study range from late Early Cretaceous to latest Eocene in age (Figure 5). The majority of ZFT ages ($n = 8$) are between ~90 and ~70 Ma, and a smaller population of ZFT ages ($n = 4$) are between ca. 65 and 50 Ma. Only two samples are outliers from these populations with ZFT ages of 34.3 ± 1.5 Ma (latest Eocene) and 115.9 ± 6.0 Ma (Aptian).

New ZHe ages include one sample with only Eocene ages, one sample with only Miocene ages, and two samples with greater single grain age variability ranging from late Eocene to Miocene. One sample with single grain variability, FPT17-23 exhibited a slight positive age-eU relationship (see Figure S1 in Supporting Information S1). No samples exhibited an age-grain size relationship (see Figure S2 in Supporting Information S1). For samples with complementary ZFT ages, the ZHe ages (new and previously published) are consistently younger than ZFT ages.

## 5. Modeling Methods

### 5.1. Thermal History Modeling

Thermal history modeling provides a quantitative comparison between the measured thermochronology data sets reported above—including cooling age (ZFT, ZHe), grain size (ZHe), and eU concentration (ZHe)—and possible time temperature histories (Abbey et al., 2023; Murray et al., 2022; Wolf et al., 1998). The thermochronometric cooling ages in this study collectively span (Aptian) Late Cretaceous through Miocene cooling (Figure 5), suggesting that modeling this data set can evaluate thermal histories during the Paleogene.

Prior to modeling, samples with both ZFT and ZHe data were screened to ensure that modeling was geologically relevant and to ensure data quality and reproducibility. For samples from intrusive rock units (e.g., batholith rocks or hypabyssal levels of the Tobífera Formation) with a ZFT date <10 Myrs younger than interpreted crystallization/emplacement age from the same sample or nearby rocks from published data sets (Hervé, Massonne, et al., 2007; Muller et al., 2021; Thomson et al., 2001), we interpreted the ZFT date as post-intrusive emplacement cooling rather than exhumation (Hervé, Massonne, et al., 2007; Muller et al., 2021; Thomson et al., 2001). Individual ZHe data were screened for single grain ZHe date reproducibility before including individual dates from single aliquot samples in thermal modeling exercises (Flowers et al., 2015; Murray et al., 2022). Additional details of data screening and input are described in Supporting Information S1 (Text S1).

Inverse modeling using HeFTy v.1.9.3 (Ketcham, 2005) generates individual, random time-temperature histories and evaluates the likelihood that each time-temperature history will produce the observed data using the goodness of fit statistic (Ketcham, 2005). Individual time-temperature (t-T) paths that do not fail the null hypothesis are described as good fit paths if all inputs (ZFT date, ZHe date(s)) score >0.5, and acceptable fit paths if all inputs score between 0.05 and 0.5. Inverse thermal models were set to run until 100 good fit paths were identified.

Inverse models were designed for each sample according to independent geologic constraints and to maximize the diversity of possible t-T paths consistent with the new thermochronology data and existing geologic constraints (Murray et al., 2022). Samples eligible for thermochronologic modeling were classified according to lithology and inferred geologic history (Table 1). A separate set of models was designed for the unique geologic histories associated with the hypabyssal/volcaniclastic rocks of the Tobífera Formation (metamorphosed and non-metamorphosed samples) and detrital clasts from upper Cretaceous strata of the Magallanes Basin (Figure S4 in Supporting Information S1). A detailed description of these model designs are included in Supporting Information S1 (Text S1).

## 6. Thermal History Modeling Results and Path Families

The individual 100 good fit t-T paths identified from inverse modeling exhibit a broad envelope across all samples including both monotonic and non-monotonic (i.e., reheating) cooling paths and variations in the timing, rate, and magnitude of heating and cooling prior to converging on a rapid cooling trend by ~20 Ma (Figure 6). These results are consistent with the design of the model to identify the most diverse suite of possible thermal histories. The non-unique thermal solutions—particularly after 70 Ma and before 20 Ma when there are few independent geologic constraints on the thermal history—make it difficult to interpret the thermal history models. We apply the Path Family Approach (Murray et al., 2022) to identify a finite subset of thermal trends within these broad results that exhibit similar timing and rates of heating and cooling events called path families (Figures 6 and 7). We focus our classification scheme on the unique thermal behaviors in the Paleogene and earliest Neogene as this is the time period with outstanding geological questions. For additional details on our use of the Path Family Approach, see Supporting Information S1 (Text S2).

Among the non-detrital samples, we identify three distinct path families, Path Families 1, 2, and 3 (Figures 6 and 7). Both detrital clast samples also resolve Path Families 1 and 3 plus an additional unique path family, Path Family 4, that captures the post-depositional history of these detrital clasts. The criteria used to define each path

**Table 1**
*Thermochronology Sample Locations and Information*

| Sample name | Latitude | Longitude | Elevation (m) | Tectonic domain | Geologic unit | Lithology | ZFT | ZHe | AFT | Modeling |
|---|---|---|---|---|---|---|---|---|---|---|
| FPT17-27 | −53.418 | −72.1541 | 0 | Western domain—RVB | Tobífera Fm. | metarhyolite | X | X | | X |
| FPT17-23 | −53.210 | −72.4830 | 22 | Western domain—RVB | Tobífera Fm. | metarhyolite | | X | | |
| FPT17-68 | −52.832 | −72.9581 | 13 | Western domain—RVB | Tobífera Fm. | metarhyolite | X | X[b] | | X |
| FPT17-62 | −52.823 | −72.8847 | 0 | Western domain—RVB | Tobífera Fm. | metarhyolite | X | X | | X |
| FPT17-59 | −52.804 | −72.8272 | 26 | Western domain—batholith | SP Batholith | diorite | X | X[b] | | |
| FPT17-55 | −52.771 | −72.7991 | 2 | Western domain—RVB | Tobífera Fm. | metarhyolite | X | X | | X |
| FPT17-49 | −52.720 | −72.7304 | 22 | Western domain—RVB | Tobífera Fm. | metarhyolite | X | X[b] | | X |
| FPT17-45 | −52.587 | −72.2328 | 8 | Central domain | Escarpada Fm. (detrital clast) | granitoid clast | X | | X[b] | X |
| 08-JF-125 | −52.100 | −73.2045 | 82 | Western domain—RVB | Tobífera Fm. | silicic volcaniclastic | X | | | |
| 08-135 | −51.562 | −74.0731 | 4 | Western domain—batholith | SP Batholith | granodiorite | X | X[a] | | |
| 08-143 | −51.451 | −73.5534 | 90 | Western domain—RVB | Tobífera Fm. | metarhyolite | X | X[a] | | X |
| 10-133 | −51.446 | −73.3482 | 23 | Western domain—batholith | SP Batholith | granodiorite | X | X[a] | | |
| 07-29 | −51.127 | −72.6772 | 876 | Central domain | Cerro Toro Fm (detrital clast) | granitoid clast | X | X[a] | | X |
| 07-116 | −51.098 | −73.3077 | 434 | Western domain—RVB | Tobífera Fm. | silicic volcaniclastic | X | X[a] | | X |
| 07-56 | −51.076 | −73.2465 | 209 | Western domain—RVB | Tobífera Fm. | rhyolite | X | X[a] | | X |

*Note*. Refer to Figure 5 for a graphical summary of cooling ages and Supporting Information S2 for fission track measurements and single grain data (U-Th)/He.
[a]Published in Fosdick et al. (2013). [b]Published in Stevens Goddard & Fosdick (2019).

family identified in this modeling exercise are described in detail below. Although the magnitude of heating and/or cooling (and thus peak or minimum temperatures reached during these periods) may vary among samples, the timing and direction of thermal change (or lack of change) satisfies the objective criteria used to define path families across samples.

*Path Family 1*: Individual t-T paths in Path Family 1 are either retained at (in the case of unmetamorphosed samples), recooled to (in the case of metamorphosed samples), or initiate at (in the case of detrital clasts) relatively cool temperatures above the ZFT closure temperature (~185–280°C) until at least 80 Ma or as late as ~20 Ma at which point, samples are reheated by at least 100°C and in some cases >300°C (Figures 6 and 7). The timing and magnitude of this reheating is considered the key classification criteria for defining this path family. Peak Cenozoic temperatures are reached as early as ca. 45 Ma, but most commonly between 35 and 20 Ma. Reheating is followed by rapid final cooling that initiates after 35 Ma or as late as ~15 Ma.

*Path Family 2*: Individual t-T paths in Path Family 2 are heated to temperatures in or above the ZFT PAZ by 80 Ma (Figures 6 and 7). Although some (but not all) paths exhibit moderate cooling between 80 and 60 Ma, after 60 Ma, all paths exhibit a period of almost no heating or cooling for a period of ca. 20–40 Myrs. The temperature at which samples were retained in the model varies across samples. In all samples, the samples resided at temperatures of at least 150°C, but several samples resided at temperatures >250°C. Retention is followed by accelerated final cooling after 35 Ma, a trend that is broadly consistent with the timing and rate of final cooling observed in Path Family 1 (Figures 6 and 7).

*Path Family 3*: Path Family 3 includes heterogeneous trends among individual t-T paths, even within samples, prior to ~50 Ma (Figures 6 and 7). Some paths are heated to relatively high temperatures (at least 150°C, but up to 300°C) with final heating at ~50 Ma. Some paths are heated to high temperatures as early as ~100 Ma and retained at high temperatures until ~50 Ma. Other paths are heated to high temperatures, cooled, and then reheated prior to ~50 Ma. However, all samples in Path Family 3 (and only in Path Family 3) exhibit an increase in the rate of cooling between 50 and 35 Ma. Cooling is most common across samples between 45 and 40 Ma (Figures 6 and 7). Some individual paths have a second phase of accelerated cooling after 35 Ma, synchronous with the post 35 Ma cooling events observed in Path Families 1 and 2.

*Path Family 4*: After foredeep deposition at surface temperatures ca. 85–80 Ma (Bernhardt et al., 2012; Daniels et al., 2019; McAtamney et al., 2011; Romans et al., 2010), individual t-T paths in Path Family 4 are quickly

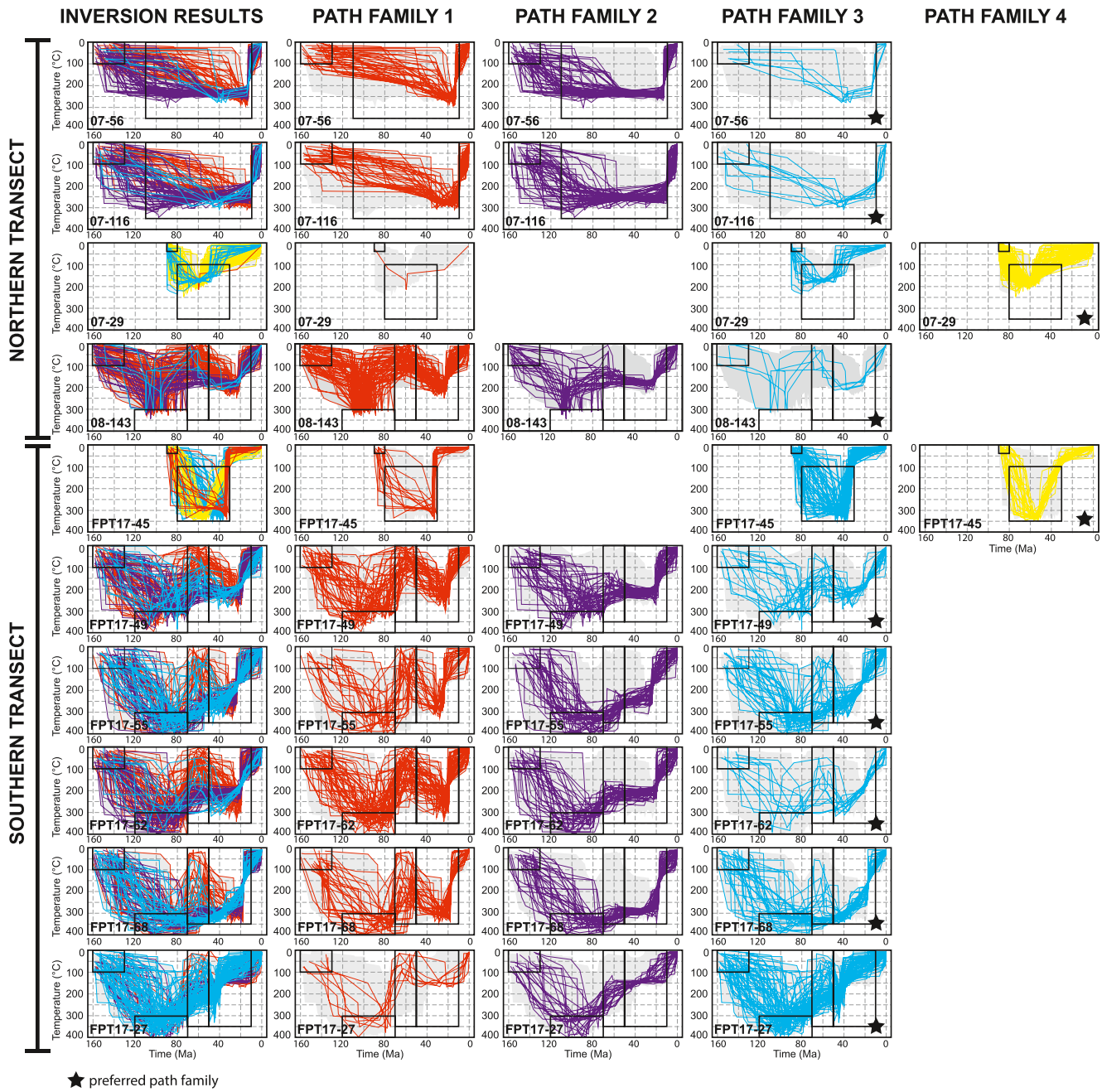


**Figure 6.** Thermal history modeling results produced using HeFTy v.1.9.3. Each inversion shows 100 good fit paths found using the inverse modeling process described in detail in the text. Black boxes indicate geologic constraints or model exploration boxes. The location of these boxes is discussed in 5.5 Model Design. In the first column, all thermal history modeling results are shown with all individual paths stacked on top of each other. Each path is color coded according to its Path Family. Path Family 1 paths are red, Path Family 2 paths are purple, Path Family 3 paths are blue, and Path Family 4 paths are yellow. The second through fifth columns show only the individual paths that are classified by the Path Family indicated at the top of each column.

reheated to temperatures within the ZFT PAZ (Figures 6 and 7). Cooling initiates between 70 and 50 Ma, and samples are cooled to temperatures above the ZHe PRZ by 45 Ma, but in most cases before 60 Ma. Some individual t-T paths have a second accelerated phase of cooling after 35 Ma, but this cooling initiates from temperatures cooler than 100°C which is lower than the closure temperatures of both the ZFT and ZHe systems. This final phase of cooling contrasts with Path Families 1, 2, and 3 in which final cooling initiates at temperatures of at least 150°C.

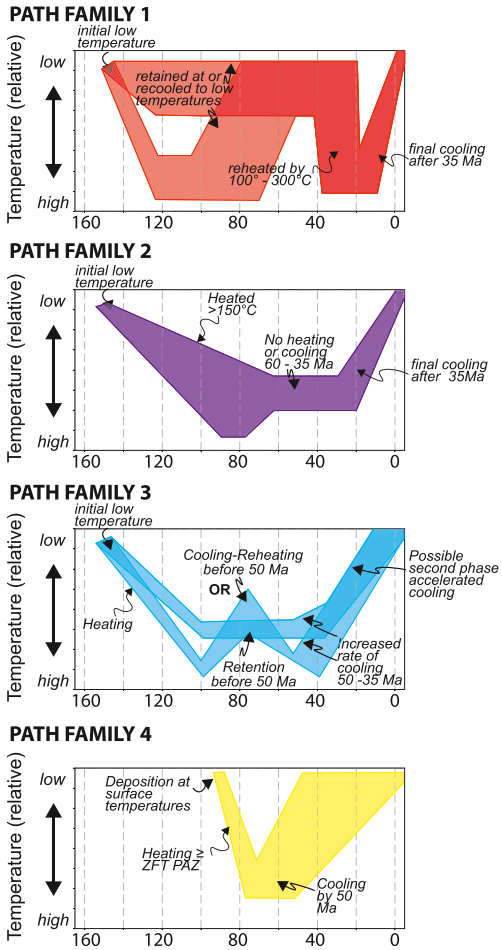


**Figure 7.** A schematic diagram shows the heating and cooling envelopes of distinct Path Families identified in the inverse modeling process. Path Families are thermally plausible solutions, but may or may not be consistent with the geologic history of a sample given the local structural location and tectonic context. Path Families 1, 2, and 3 are identified for all non-detrital samples. Path Families 1, 3, and 4 are identified for all detrital samples (Cretaceous clastic strata). Path Families 1 and 3 both show two component subpopulations that, despite minor differences, share the common thermal behaviors in the Paleogene–Neogene used for the classification scheme in this study.

## 7. Evaluation of Path Families in the Context of Southern Patagonia

The thermochronology data generated in this study are consistent with multiple path families that represent different possible geologic histories (Figures 6 and 7). Using thermochronology data alone, we would be unable to select a preferred path family as all solutions are thermally plausible; however, we can eliminate path families that are inconsistent with the geologic history of Patagonia based on other geologic information. We also consider the inter-sample compatibility of thermal histories given the local structural context and/or tectonic environment. Evaluation of path families considers both the thermal processes that may produce the unique thermal conditions of each path family and the geologic context of the southern Patagonian Andes during the Paleogene through earliest Neogene.

The thermal history of a modeled data set limits subsequent thermal behaviors, thus, if one modeled thermal event is geologically implausible, then it invalidates the entire thermal history of the modeled t-T path. We focus our evaluation of Path Families on the unique and contradictory thermal trends observed among each Path Family between ca. 60 and 20 Ma. For example, during this period of time, Path Family 1 requires heating of 100°–300°C, Path Family 2 requires samples to stay at a nearly constant temperature, Path Family 3 requires a 50–35 Ma cooling signal that does not occur in other Path Families, and Path Family 4 requires samples to start cooling to near-surface temperatures before 50 Ma (Figures 6 and 7). Each path family has a unique thermal signature between 60 and 20 Ma.

The geologic context of the thermal trends provided for each path family enables us to evaluate the plausibility of each path family and eliminate some path families altogether. For example, Path Family 1 requires high magnitude heating and cooling. The timing, rate and magnitude of this thermal history is not consistent with geologic processes in this tectonic setting. Likewise, Path Family 2 requires sustained thermal stasis for 40–20 Myrs, thermal conditions that are likely in a stable intracontinental setting, but uncommon at active plate margins. An expanded evaluation of Path Families is provided in Supporting Information S1 (Text S2).

We describe the preferred path families for the samples in our study. Although existing geologic context governs our selections of preferred path families, the thermal trends identified in these preferred path families provide new insight into the location, timing, and style of the processes that are preserved in these thermal signatures (addressed in Section 8). For samples of the Tobífera Formation located in the western thrust belt domain (Figures 1 and 2), we prefer Path Family 3. Metamorphosed samples in this domain reach peak temperatures >300°C by model design, a reflection of interpreted tectonic emplacement of ophiolitic complexes (e.g., Calderón et al., 2012; Muller et al., 2021); however, unmetamorphosed samples from the basement thrust belt, 07–56 and 07–116 from the northern transect, also require samples to reach peak temperatures between 250 and 300°C prior to 50–35 Ma cooling (Figures 6 and 7). The consistency in magnitude and timing of peak heating across samples is consistent with sediment burial in the post-rift phase of the RVB (e.g., Zapata/Erezcano Formations) and Cretaceous foreland basin strata, but does not preclude tectonic burial. The start of a cooling phase between 50 and 35 Ma is geologically consistent with enhanced erosion of an active thrust belt—an Eocene deformation event suggested by kinematic reconstructions, but poorly constrained spatially and temporally (P. Betka et al., 2015; Fosdick et al., 2011; Ghiglione et al., 2014; Klepeis et al., 2010). This preferred interpretation assumes erosion is sufficient to cool samples across the thrust sheet (Metcalf et al., 2009; ter Voorde et al., 2004). Importantly, cooling that begins between 50 and 35 Ma is maintained through the Neogene with accelerated cooling in the Miocene (Stevens Goddard & Fosdick, 2019; Thomson et al., 2010) suggesting that the mechanism responsible for initial cooling and interpreted erosion is

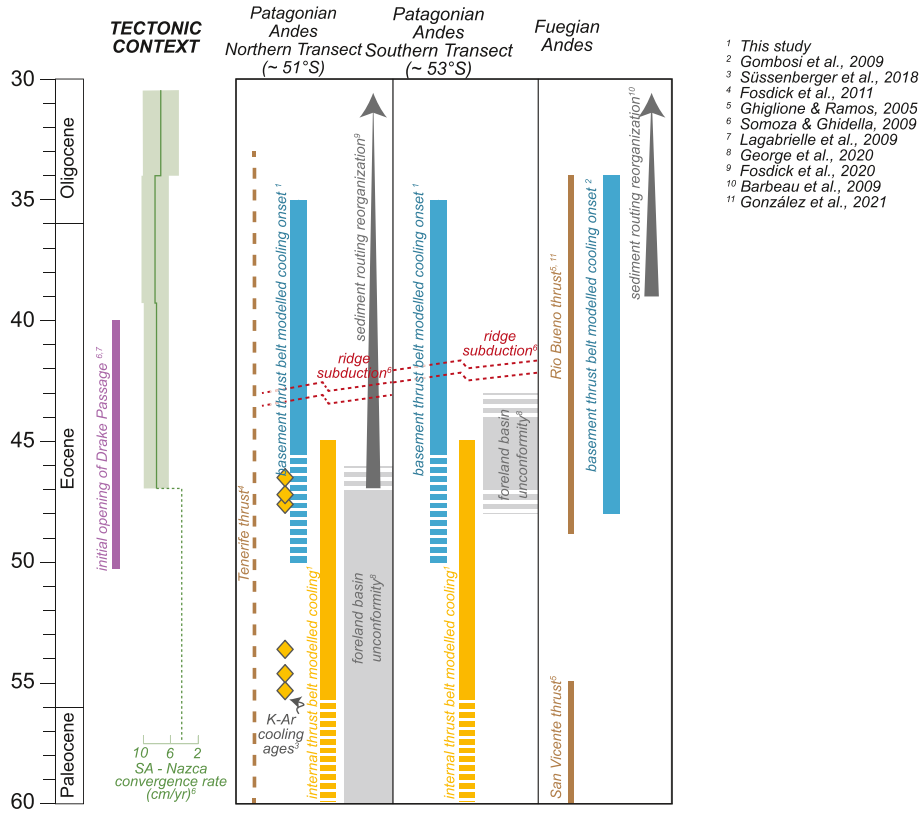


**Figure 8.** Temporal summary diagram from this study and published work of timing of modeled cooling, deformation, sedimentation hiatuses and reorganizations, and ridge subduction for the northern and southern transects referenced in this study for the southern Patagonian Andes and the Fuegian Andes. Local geologic records in the right three columns are compared with global plate convergence rates and the timing of the opening of the Drake Passage. Results from this study highlight that cooling onset across the southern Patagonian and Fuegian Andean systems occur simultaneously with a change in sediment routing suggesting a period of thrust belt deformation (cooling produced by enhanced exhumation and erosion) that reorganizes drainage systems during the initial opening of the Drake Passage.

continuous or overlaps with younger erosional episodes. We note that Path Family 3 is also consistent with a phase of Late Cretaceous exhumation associated with retroarc shortening, but the precision of the model results for this time period are not sufficient to analyze the timing or magnitude of cooling rigorously.

For Upper Cretaceous conglomerate samples located in the central thrust belt domain, we prefer Path Family 4 over Path Family 3 for two reasons. First, the timing of cooling associated with Path Family 4, most likely by 60 Ma, is consistent with the stratigraphic record of the regional Paleogene unconformity preserved in the foreland basin strata (Biddle et al., 1986; Fosdick et al., 2011, 2015; George et al., 2020; Sickmann et al., 2018). Second, although contemporaneous out-of-sequence deformation in both the basement thrust belt and the central thrust belt domain is possible, there is less evidence that deformation stepped out to the central thrust belt domain until at least the Oligocene (Fosdick et al., 2011, 2013).

## 8. Discussion

### 8.1. Thermochronological Record of Eocene Thrust Belt Deformation and Implications for Along-Strike Deformation

Although the Late Cretaceous and Neogene episodes of Andean deformation in the western thrust belt domain of the southern Patagonian Andes have been well-documented at the latitudes of our study area, ~51°–53°S (Figure 8), the Paleogene chronology of orogenesis has remained largely enigmatic (P. Betka et al., 2015; Calderón et al., 2012; Fosdick et al., 2011; Ghiglione & Ramos, 2005; Ghiglione et al., 2009; Klepeis, 1994; Süssenberger et al., 2018; Wilson, 1991). Fosdick et al. (2011) document contractional deformation of the western

thrust belt domain in the Ultima Esperanza district (~51°S–51.5°S), but only broadly constrain this deformation using cross-cutting relationships to between 74 and 27 Ma. Süssenberger et al. (2018) interpret K-Ar dates from authigenic illites near mapped faults in the same region as an episode of enhanced regional uplift caused by out-of-sequence deformation starting by at least the earliest Eocene (Figure 8). Provenance records from Paleogene foreland basin strata between 51° and 51.5°S document a change in drainage organization that Fosdick et al. (2020) interpret as an Eocene phase of hinterland thrust belt deformation beginning ca. 47 Ma (Figure 8). South of the Ultima Esperanza district, a chronometric data gap that extends into the Fuegian Andes provides few constraints on Paleogene deformation history (P. Betka et al., 2015; Ghiglione & Ramos, 2005; Klepeis & Austin, 1997; Torres Carbonell et al., 2020).

The results from this study provide new thermochronologic data that confirm the occurrence of an Eocene thermotectonic event between ~51°S and 53°S that is best explained by a phase of Eocene deformation in the western thrust belt domain (Figure 8). Preferred path families document a cooling trend in basement thrust belt samples from both hanging wall and footwall positions between ca. 50 and 35 Ma, with cooling most common between ca. 45 and 40 Ma (Figures 5–7). The spatiotemporal pattern of cooling observed in the preferred path families can best be explained by erosion and exhumation of thrust sheets (e.g., Metcalf et al., 2009; ter Voorde et al., 2004). The relative synchronicity of this cooling both across and along strike is consistent with the cooling patterns expected from out-of-sequence deformation.

Notably, cooling observed from the thermal history models in this study is slightly younger than the earliest K-Ar cooling ages from authigenic illite identified by Süssenberger et al. (2018), which are between ca. 55 and 45 Ma (Event 4; Figure 8). However, the K-Ar closure temperature of ~320 ± 20°C—appropriate for the mineral phase and grain fraction reported by Süssenberger et al. (2018) Pevear (1992), Środoń et al. (2002)—is higher than the closure temperature of the ZFT system (Bernet, 2009; Ketcham, 2019; Zaun & Wagner, 1985). This result may suggest that cooling constrained by the preferred path family (Path Family 3) in this study captures the continuation of a cooling trend which is recognized slightly earlier and at higher temperatures by the K-Ar system. Alternatively, the K-Ar cooling ages classified by Süssenberger et al. (2018) as a single event may represent two discrete cooling events, the first ca. 55–53 Ma. and the second ca. 48–46 Ma.

Earliest cooling observed in the western thrust belt domain using thermal history models ca. 50 Ma is contemporaneous with a change in provenance recognized at ca. 47 Ma (Fosdick et al., 2020) suggesting there is a tight connection between basement thrust belt deformation and the reorganization of foreland basin sediment routing patterns. It is notable that drainage reorganization also closely overlaps with a subset of ca. 48–46 Ma K-Ar cooling ages measured by Süssenberger et al. (2018) suggesting that this data set may indeed record two discrete events (Figure 8).

The results of this study corroborate the observations and interpretations of Fosdick et al. (2011, 2020) and Süssenberger et al. (2018) of an Eocene phase of orogenesis associated with out-of-sequence deformation in the Ultima Esperanza district and provide the first evidence that the timing and style of deformation observed in this region extends to latitudes ~53°S within the southernmost Patagonian thrust belt (Figure 8). Moreover, these results resolve an Eocene deformational event that has long been recognized kinematically at latitudes 51°–53°S, but has been poorly dated. Specifically, we suggest 50–35 Ma Tenerife out-of-sequence thrusting and rotation of Tobífera thrusts (Fosdick et al., 2011). This finding is significant as it requires deformation and growth of the southern Patagonian Andes during a period thought to be characterized by deformational quiescence along much of the margin (Horton, 2018). The start of Eocene deformation in the southern Patagonian Andes precedes spreading ridge subduction as reconstructed by plate kinematic models suggesting spreading ridge subduction does not drive deformation in the thrust belt.

This new evidence for Eocene orogenesis along the southern Patagonian Andes has important implications for the co-evolution of the southern Patagonian Andes and the Fuegian Andes (Figure 8). Unlike in the southern Patagonian Andes, Eocene deformation in the Fuegian Andes has been well documented and dated (Barbeau et al., 2009; Ghiglione & Ramos, 2005; Ghiglione et al., 2010; Klepeis, 1994). In Tierra del Fuego, cratonward thrust belt propagation is dated using field relationships and basinal unconformities to between 49 and 34 Ma (Barbeau et al., 2009; Biddle et al., 1986; Ghiglione & Ramos, 2005; Ghiglione et al., 2010; Klepeis, 1994; Malumián & Olivero, 1998; Olivero et al., 2001; Torres Carbonell et al., 2008). Ar-Ar and ZFT data sets document exhumation of the Cordillera Darwin complex at ca. 50 Ma (Kohn et al., 1995; Nelson, 1982), and integrated thermal history modeling of ZFT, ZHe, AFT, and AHe data sets from the Cordillera Darwin complex as

well as rocks from the Tobífera Formation resolve a period of accelerated cooling that begins as early as 48 Ma and ends by 34 Ma (Gombosi et al., 2009), nearly identical in timing with the modeled cooling in this study. These cooling signals in the Fuegian Andes are widely interpreted as accelerated exhumation and erosion associated with a distinct phase of orogenesis (Ghiglione & Ramos, 2005; Gombosi et al., 2009; Klepeis et al., 2010; Kohn et al., 1995). Barbeau et al. (2009) use provenance analysis from detrital zircons to identify a shift in the drainage organization of the foreland basin system associated with the Fuegian Andes at ca. 39 Ma that is interpreted as a contemporaneous response to uplift and shortening in the Fuegian thrust belt system at this time (Figure 8).

Thermochronological results from deformational centers in both the southern Patagonian Andes (this study) and the Fuegian Andes (Gombosi et al., 2009; Kohn et al., 1995; Nelson, 1982) identify a common phase of Eocene orogenesis from ca. 50–35 Ma that corresponds to a phase of foreland basin drainage reorganization in each system (Barbeau et al., 2009; Fosdick et al., 2020; Torres Carbonell & Olivero, 2019). These results may suggest that in the Eocene, the southern Patagonian Andes and the Fuegian Andes were part of an active, connected Cordilleran retroarc compressional system along the bend of the Patagonian orocline. Most workers concur that the Patagonian orocline is either a primary arc or a curved belt formed by secondary bending already developed by 50 Ma (Maffione et al., 2010), prior to the Eocene phase of orogenesis identified in this study (Eagles, 2016; Ghiglione & Cristallini, 2007; Kraemer, 2003; Poblete et al., 2014). The curved orogen shape would require simultaneous E-W (Patagonian Andes) and N-S (Fuegian Andes) directed shortening. Strike-slip deformation along local or regional restraining bends within the Magallanes Fagnano fault zone could produce compressional deformation (P. Betka et al., 2022), however, this system did not commence until the Oligocene (P. Betka et al., 2016; Ghiglione & Ramos, 2005; Klepeis, 1994). Although the thermochronology data in this study does not constrain the magnitude of Eocene shortening within the system between 51° and 53°S, previous work documenting the kinematics of deformation support an increase in the magnitude of shortening southward in the southern Patagonian system toward the transition to the Fuegian Andes (P. Betka et al., 2015; Fosdick et al., 2011; Ghiglione & Ramos, 2005; Ghiglione et al., 2010; Klepeis, 1994). Plate reorganization at 50 Ma of the South American, Scotia, and Antarctic Plates (Eagles, 2016; Scher & Martin, 2006) may simply have facilitated subduction zone conditions (increased convergence rates, increased plate coupling, shallow slab angle) amenable to retroarc contraction (Horton, 2018; Somoza & Ghidella, 2012) that wrapped around the curved orogen along the Antarctic–South American plate subduction zone (Maloney et al., 2013). Alternatively, N-S directed shortening in the Fuegian Andes may have propagated stress into the southern Patagonian system that was accommodated on pre-existing N-S striking structures in the southern Patagonian Andes as far north as 51°S. In either case, plate reorganization associated with the early opening of the Drake Passage at 50 Ma can be linked to retroarc compressional deformation in the southern Patagonian Andes. North of our study area, ~48–44°S, AHe, AFT, ZHe, and ZFT data sets and thermal history models incorporating AFT and ZHe data sets do not show evidence of Eocene–Oligocene exhumation and inferred deformation (Georgieva et al., 2016; Guillaume et al., 2013; Ronda et al., 2022; Thomson et al., 2001, 2010). It is possible that thermal history modeling incorporating data from a higher temperature thermochronometric system is required to identify this signal. Alternatively, the absence of this signal could indicate that the deformation did not reach this far north.

### 8.2. Orogen-Basin Connections for the Paleogene Unconformity Development

During periods of both deformation and quiescence, thrust belts and foreland basins in Cordilleran systems are genetically linked (DeCelles & DeCelles, 2001; Horton, 2018; Jordan, 1995; Xie & Heller, 2009). Crustal shortening and uplift in the thrust belt produces flexural subsidence of the foreland basin that is filled by eroded materials in the topographically emergent thrust belt (DeCelles & Giles, 1996; Dickinson, 1974; Jordan, 1995). In the absence of upper plate stress, the adjacent fossil thrust belt and foreland (along with other adjacent tectonomorphic regions such as the batholith) are subjected to shared geodynamics common along Cordilleran plate margins—for example, the subduction of buoyant crust, slab-induced suction, or modified mantle flow patterns (e.g., Dávila & Lithgow-Bertelloni, 2013, 2015; Dávila et al., 2018; Delph et al., 2021; Furlong & Govers, 1999)—that drive long-wavelength uplift and subsidence. In these scenarios, uplift and subsidence occur across both the thrust belt and the foreland. The inherently linked response to tectonic and geodynamic processes between the thrust belt and foreland basin allows us to reevaluate the mechanism responsible for the Paleogene unconformity observed in the Magallanes-Austral basin in the context of our new thermochronology data (Figure 3). Specifically, we use our bedrock thermochronology data to compare the presence and timing of cooling and interpreted erosion in the western and central thrust belt domains with the time period represented by the unconformity in the foreland

basin, spanning between ca. 65–60 Ma and 47–45 Ma, at the latitudes of our study area (Biddle et al., 1986; Fosdick et al., 2015, 2020; George et al., 2020; Ghiglione et al., 2016; Horton, 2022; Malumián et al., 2000; Sickmann et al., 2018).

The ZFT data from batholith rocks in the western thrust belt domain preserve magmatic cooling signals indicating that total erosion was less than ∼10 km since the Cretaceous (Figure 5). Reproducible ZHe data from batholith samples preserve latest Oligocene–early Miocene cooling ages. Although batholith thermochronology data were not modeled, the ZFT and ZHe cooling ages suggest that more erosion of batholith rocks occurred after the end of the Paleogene unconformity, consistent with previous interpretations of batholith erosion (Fosdick et al., 2013; Thomson et al., 2001, 2010) and that less erosion of the batholith occurred during formation of the Paleogene unconformity.

In the metasedimentary and hypabyssal RVB rocks of the western thrust belt domain (Figure 1), the preferred path family model (Path Family 3) resolves cooling between ca. 50 and 35 Ma, (Figures 6 and 7) suggesting inferred exhumation continued long after sedimentation resumed in the foreland basin system at 47–45 Ma (Figure 8). These orogen-basin observations imply that 50–35 Ma cooling in the basement thrust belt is not mechanistically linked to foreland erosion responsible for Paleocene unconformity (Figure 3). This is consistent with our interpretation that cooling is instead related to out-of-sequence contractional deformation (Section 8.1) that would produce subsidence (rather than uplift) in the foreland. If the K-Ar cooling ages from Süssenberger et al. (2018) do indeed resolve two separate cooling events, it is possible that the 55–53 Ma K-Ar cooling ages in the western thrust belt domain may reflect rock cooling associated with widespread Paleocene erosion; however the magnitude of erosion, if it indeed exists, is difficult to resolve.

Farther east, the preferred thermal history (Path Family 4) for the Upper Cretaceous conglomerate clasts within the central thrust belt domain requires burial heating and rapid cooling that commenced between ca. 60–50 Ma. Within this preferred thermal history, individual paths can cool to temperatures at or above the closure temperature of the ZHe system by ca. 45 Ma, a thermal solution which is not possible for samples from the basement thrust belt. We suggest that 60–50 Ma cooling observed in the deformed Cretaceous basinal strata of the central thrust belt domain provides direct evidence that cooling and inferred erosion associated with the Paleogene foreland basin unconformity extended to the central thrust belt domain, which was likely the eastern edge of the thrust belt at the time (Biddle et al., 1986; Fosdick et al., 2015, 2020; George et al., 2020; Ghiglione et al., 2016; Horton, 2022; Malumián et al., 2000; Sickmann et al., 2018). It would be ideal to use this data set to interrogate the time that erosion started, but the preferred path family envelope is insufficiently narrow (Figures 6 and 7) and includes solutions in which cooling starts as early as 60 Ma or as late as 50 Ma, and thus it is not possible to resolve the initiation of erosion within the time period represented in the foreland basin unconformity.

The thermochronology data from the western domain including batholith rocks and RVB rocks (Tobífera thrust sheets) as well as deformed Upper Cretaceous foreland strata of the central domain, suggests that the areas affected by erosion at the same time as the Paleogene unconformity corresponds to boundaries between tectonomorphic domains (Figure 8). Specifically, synchronous Eocene erosion extended from the proximal foredeep to the structural margins of the thrust belt (central thrust belt domain, in present-day localities). This observation alone is not sufficient to isolate a single mechanism driving the erosional event represented by the Paleogene unconformity, but it does enrich assessments of the erosional mechanisms driving unconformity development and eliminate some hypotheses discussed below (George et al., 2020; Horton, 2022). The large scale magnitude and timing (regionally diachronous, millions to tens of millions of years) of the Paleogene unconformity, in addition to its angular stratal geometry in many places (Fosdick et al., 2020; Torres Carbonell et al., 2020), require a mechanism beyond eustatic sea level fall and subaerial exposure of the basin floor. The absence of erosion across all tectonomorphic domains excludes Eocene erosional decay associated with tectonic quiescence along a neutral plate margin (Horton, 2018, 2022) and instead provides evidence of active tectonic or geodynamic processes. It is possible that changes in thrust wedge geometry through either internal deformation or forward propagation facilitated erosion in the external thrust belt without generating a sufficient load to sustain foreland subsidence (Davis et al., 1983; DeCelles & Mitra, 1995). An Eocene hiatus in arc magmatism (Hervé, Massonne, et al., 2007; Ramos, 1989) may provide evidence that erosion was caused by modified crustal stresses or geodynamic conditions associated with flat slab subduction (Dávila & Lithgow-Bertelloni, 2015; Dávila et al., 2010) or Farallon-Aluk spreading ridge subduction (Cande & Leslie, 1986; Eagles & Scott, 2014; Ramos, 2005; Somoza & Ghidella, 2012). However, each of these hypotheses are made controversial in light of other geologic

observations including, respectively, the absence of high-angle deformation in the foreland basin (a hallmark of flat-slab subduction; Jordan & Allmendinger, 1986; Ramos & Folguera, 2009; Yonkee & Weil, 2015) and resumed sedimentation before passage of the Farallon-Aluk spreading ridge. Although not diagnostic, our data provide a strategic starting point for additional targeted geologic data sets and geodynamic experiments that could interrogate the cause of unconformity development.

### 8.3. Thermal Insights Into Sediment Burial in the Patagonian Foreland Basin

The thermal history data and modeling exercises in this study can help reconstruct the volume of eroded material that was deposited across the southern Patagonian foreland. Conglomerate clasts extracted from Upper Cretaceous strata in the central thrust belt domain are a particularly useful indicator of the thermal history of the foreland basin. Both detrital clasts in this study preserve ZFT and ZHe ages that are younger than the depositional age of host strata. This suggests that burial by overlying Upper Cretaceous–Paleocene foreland basin strata produced sufficient heating to fully or partially reset the ZFT and ZHe systems (Daniels et al., 2019; Ghiglione et al., 2014; McAtamney et al., 2011; Romans et al., 2011; Schwartz & Graham, 2015; Sickman et al., 2018; Wilson, 1991). Thermal history models of these samples enable a reconstruction of past peak thermal conditions which can be used to evaluate variations in the thickness of Magallanes-Austral foreland basin sediments along strike. Thermal models for sample 07–29 from the northern transect require the sample to reach peak post-depositional temperatures between 150 and 200°C. In contrast, thermal models for FPT17-45 from the southern transect require the sample to reach peak post-depositional temperatures of >300°C. Assuming a geothermal gradient of 30°C/km (Fosdick et al., 2015), these models indicate that there is a difference of ∼3–5 km of Upper Cretaceous–Paleocene sediment burial between the two locations.

This discrepancy could be caused by a difference in proximity to the active thrust front in the foreland basin system (DeCelles & Giles, 1996). Samples 07–29 and FPT 17–45 are located ∼25 and ∼10 km from this structural boundary, respectively (Figure 3). However, flexural models of the Late Cretaceous foredeep suggest that a difference of only ∼15 km from the thrust front is not consistent with the required variation in sediment thickness (Fosdick et al., 2014). Alternatively, these differences in peak burial temperatures could reflect a change in basin thickness along strike as has been represented in classic isopach maps by Biddle et al. (1986). Paleocurrent measurements from Upper Cretaceous basin strata document a shift from southward-directed axial sediment transport north of ∼52°S that transitions to transverse sediment transport by ∼53°S (Armitage et al., 2009; Covault et al., 2009; Fildani & Hessler, 2005; Ghiglione et al., 2019; Hubbard et al., 2008; Katz, 1963; Malkowski et al., 2016; McAtamney et al., 2011; Romans et al., 2011; Scott, 1966; Winn & Dott, 1979). In the Ultima Esperanza District (∼51°S–51.5°S), Schwartz et al. (2017) document increased aggradation rates in Campanian foreland strata that are followed by an increase in southward progradation as the northern foreland basin filled. In this scenario, sediment bypassed local depocenters in the northern part of the basin and was deposited in the south producing a southward deepening foreland sequence. A southward increase in shortening magnitudes in the thrust belt also supports this matched increase in accommodation space to the south (P. Betka et al., 2015; Fosdick et al., 2011, 2013; Ghiglione et al., 2019; Kraemer, 1998; Ramos & Ghiglione, 2008; Wilson, 1991). Our results are consistent with this hypothesis; however more work is needed to document variations in sediment thicknesses throughout the Magallanes-Austral foreland basin system and reconstruct sediment routing pathways.

## 9. Conclusion

New thermochronologic data sets in the southern Patagonian Andes (51°S–53°S) preserve late Mesozoic—early Cenozoic spatio-temporal heating and cooling signatures that inform the timing and distribution of deformation, sedimentation, and erosion across the western and central thrust belt domains. Modeled cooling in the western thrust belt domain supports a newly recognized period of orogenesis at these latitudes between ca. 50 and 35 Ma. This deformational event is synchronous with a well-recognized phase of orogenesis in the Fuegian Andes suggesting that deformation in the southern Patagonian and Fuegian Andes was genetically linked to plate boundary organization and was continuous along the bend of the Patagonian orocline. Modeled cooling contemporaneous with the Paleogene foreland basin unconformity was only identified in the central thrust belt domain suggesting that the mechanism driving unconformity development either follows tectonomorphic boundaries or that the magnitude is significantly different across domains and is undetectable at the resolution of the data sets in this study. Modeled heating of Upper Cretaceous conglomerate clasts in the latest Cretaceous—early

Paleocene reveals a difference in peak burial temperatures that increases southward. This observation could support a southward thickening of the Late Cretaceous Magallanes basin system with an additional 3–5 km of sediment deposited in the southern basin. Thermochronology data from the Patagonian batholith reveals limited heating or cooling following emplacement indicative of tectonic stability and resistance to erosion of batholith rocks until the Neogene.

The Paleogene tectonic history of the southern Patagonian Andes has long been difficult to resolve in part due to missing stratigraphy or complex chronometric data sets. Thermal history models in this study incorporated ZFT, ZHe, and AFT thermochronometric systems to resolve a set of possible thermal histories, classified according to the Path Family Approach, that could explain the measured thermochronometric data sets. The elimination of geologically implausible time-temperature conditions allowed this study to access thermal histories consistent with the measured data sets and provide new insights on the geologic history of the southern Patagonian Andes.

## Data Availability Statement

New data presented in this work is available in the Geochron database (https://www.geochron.org/). Published data from Fosdick et al. (2013) and Stevens Goddard & Fosdick (2019) can be found in associated supplemental files.

**Acknowledgments**
Funding was provided to A. Stevens Goddard through the University of Connecticut. Field work for this project was funded in part by FONDECYT Grants 1161818 and 1211906 to M. Calderón. We thank V. Astarte Muller and K. E. Murray for conversations on Patagonian geology and thermochronologic modeling. V. Astarte Muller, C. Ramírez de Arellano, D. Rojo, M.F. Torres-García, and the crew of the *Marypaz II* provided field assistance. The authors appreciate editorial handling by Eva Enkelmann as well as though constructive feedback from Paul Betka and an anonymous reviewer which greatly improved this manuscript.

## References

Abbey, A. L., Wildman, M., Stevens Goddard, A. L., & Murray, K. E. (2023). Thermal history modeling techniques and interpretation strategies: Applications using QTQt. *Geosphere*, *18*(2), 493–530. https://doi.org/10.1130/GES02528.1

Albano Garcia, J. F., Lombardi, L., Rocha, E., Tobal, J., Fosdick, J. C., Stevens Goddard, A. L., et al. (2023). Tectonic evolution of the eastern margin of the southern Patagonian Andes fold-thrust belt: U-Pb detrital zircon geochronology and kinematic-structural modeling. *Tectonophysics*, *848*, 229705. https://doi.org/10.2139/ssrn.4153675

Angiboust, S., Cambeses, A., Hyppolito, T., Glodny, J., Monié, P., Calderón, M., & Juliani, C. (2018). A 100-m.y.-long window onto mass-flow processes in the Patagonian Mesozoic subduction zone (Diego de Almagro Island, Chile). *Bulletin of the Geological Society of America*, *130*(9–10), 1439–1456. https://doi.org/10.1130/B31891.1

Armitage, D. A., Romans, B. W., Covault, J. A., & Graham, S. A. (2009). The influence of mass-transport-deposit surface topography on the evolution of Turbidite architecture: The Sierra Contreras, Tres Pasos formation (Cretaceous), southern Chile. *Journal of Sedimentary Research*, *79*(5), 287–301. https://doi.org/10.2110/jsr.2009.035

Barbeau, D. L., Gombosi, D. J., Zahid, K. M., Bizimis, M., Swanson-Hysell, N., Valencia, V., & Gehrels, G. E. (2009). U-Pb zircon constraints on the age and provenance of the Rocas Verdes basin fill, Tierra del Fuego, Argentina. *Geochemistry, Geophysics, Geosystems*, *10*(12), Q12001. https://doi.org/10.1029/2009GC002749

Bernet, M. (2009). A field-based estimate of the zircon fission-track closure temperature. *Chemical Geology*, *259*(3–4), 181–189. https://doi.org/10.1016/j.chemgeo.2008.10.043

Bernhardt, A., Jobe, Z. R., Grove, M., & Lowe, D. R. (2012). Palaeogeography and diachronous infill of an ancient deep-marine foreland basin, Upper Cretaceous Cerro Toro Formation, Magallanes Basin. *Basin Research*, *24*(3), 269–294. https://doi.org/10.1111/j.1365-2117.2011.00528.x

Betka, P., Klepeis, K., & Mosher, S. (2015). Along-strike variation in crustal shortening and kinematic evolution of the base of a retroarc fold-and-thrust belt: Magallanes, Chile 53°S-54°S. *Bulletin of the Geological Society of America*, *127*(7–8), 1108–1134. https://doi.org/10.1130/B31130.1

Betka, P., Klepeis, K., & Mosher, S. (2016). Fault kinematics of the Magallanes-Fagnano fault system, southern Chile an example of diffuse strain and sinistral transtension along a continental transform margin. *Journal of Structural Geology*, *85*, 130–153. https://doi.org/10.1016/j.jsg.2016.02.001

Betka, P., Mosher, S., & Klepeis, K. (2022). Progressive Development of a Distributed Ductile Shear Zone beneath the Patagonian Retroarc Fold-Thrust Belt, Chile. *Lithosphere*, *2022*(1). https://doi.org/10.2113/2022/3820115

Betka, P. M. (2013). *Structure of the Patagonian fold-thrust belt in the Magallanes region of Chile, 53°–55°S*. LAT University of Texas.

Biddle, K. T., Uliana, M. A., Mitchum, R. M., Jr., Fitzgerald, M. G., & Wright, R. C. (1986). *The stratigraphic and structural evolution of the central and eastern Magallanes Basin, southern South America* (Vol. 8, pp. 41–61). Special Publication International Association of Sedimentologists. https://doi.org/10.1002/9781444303810

Calderón, M. N., Fildani, A., Hervé, F., Fanning, C. M., Weislogel, A., & Cordani, U. (2007). Late Jurassic bimodal magmatism in the northern sea-floor remnant of the Rocas Verdes basin, southern Patagonian Andes. *Journal of the Geological Society*, *164*(5), 1011–1022. https://doi.org/10.1144/0016-76492006-102

Calderón, M. N., Fosdick, J. C., Warren, C., Massonne, H. J., Fanning, C. M., Cury, L. F., et al. (2012). The low-grade Canal de las Montañas Shear Zone and its role in the tectonic emplacement of the Sarmiento Ophiolitic complex and Late Cretaceous Patagonian Andes orogeny, Chile. *Tectonophysics*, *524–525*, 165–185. https://doi.org/10.1016/j.tecto.2011.12.034

Calderón, M. N., Hervé, F., Fuentes, F., Fosdick, J. C., Sepúlveda, F., & Galaz, G. (2016). Geodynamic evolution of the southernmost Andes. https://doi.org/10.1007/978-3-319-39727-6

Cande, S. C., & Leslie, R. B. (1986). Late Cenozoic tectonics of the southern Chile trench. *Journal of Geophysical Research*, *91*(B1), 471–496. https://doi.org/10.1029/jb091ib01p00471

Christeleit, E. C., Brandon, M. T., & Shuster, D. L. (2017). Miocene development of alpine glacial relief in the Patagonian Andes, as revealed by low-temperature thermochronometry. *Earth and Planetary Science Letters*, *460*, 152–163. https://doi.org/10.1016/j.epsl.2016.12.019

Covault, J. A., Romans, B. W., & Graham, S. A. (2009). Outcrop expression of a continental-margin-scale shelf-edge delta from the Cretaceous Magallanes basin, Chile. *Journal of Sedimentary Research*, *79*(7–8), 523–539. https://doi.org/10.2110/jsr.2009.053

Dalziel, I. W. D., de Wit, M. J., & Palmer, K. F. (1974). Fossil marginal basin in the southern Andes. *Nature*, *250*(5464), 291–294. https://doi.org/10.1038/250291a0

Daniels, B. G., Hubbard, S. M., Romans, B. W., Malkowski, M. A., Matthews, W. A., Bernhardt, A., et al. (2019). Revised chronostratigraphic framework for the Cretaceous Magallanes-Austral Basin, Última Esperanza Province, Chile. *Journal of South American Earth Sciences*, *94*, 102209. https://doi.org/10.1016/j.jsames.2019.05.025

Dávila, F. M., & Lithgow-Bertelloni, C. (2013). Dynamic topography in South America. *Journal of South American Earth Sciences*, *43*, 127–144. https://doi.org/10.1016/j.jsames.2012.12.002

Dávila, F. M., & Lithgow-Bertelloni, C. (2015). Dynamic uplift during slab flattening. *Earth and Planetary Science Letters*, *425*, 34–43. https://doi.org/10.1016/j.epsl.2015.05.026

Dávila, F. M., Lithgow-Bertelloni, C., & Giménez, M. (2010). Tectonic and dynamic controls on the topography and subsidence of the Argentine Pampas: The role of the flat slab. *Earth and Planetary Science Letters*, *295*(1–2), 187–194. https://doi.org/10.1016/j.epsl.2010.03.039

Dávila, F. M., Lithgow-Bertelloni, C., Martina, F., Ávila, P., Nóbile, J., Collo, G., et al. (2018). Mantle influence on Andean and pre-Andean topography (pp. 363–385). https://doi.org/10.1007/978-3-319-67774-3_15

Davis, D., Suppe, J., & Dahlen, F. A. (1983). Mechanics of fold-and-thrust belts and accretionary wedges. *Journal of Geophysical Research*, *88*(B2), 1153–1172. https://doi.org/10.1029/jb088ib02p01153

DeCelles, P. G., & DeCelles, P. C. (2001). Rates of shortening, propagation, underthrusting, and flexural wave migration in continental orogenic systems. *Geology*, *29*(2), 135–138. https://doi.org/10.1130/0091-7613(2001)029<0135:ROSPUA>2.0.CO;2

DeCelles, P. G., Ducea, M. N., Kapp, P., & Zandt, G. (2009). Cyclicity in Cordilleran orogenic systems. *Nature Geoscience*, *2*(4), 251–257. https://doi.org/10.1038/ngeo469

DeCelles, P. G., & Giles, K. A. (1996). Foreland basin systems. *Basin Research*, 105–123. https://doi.org/10.1046/j.1365-2117.1996.01491.x

DeCelles, P. G., & Mitra, G. (1995). History of the Sevier orogenic wedge in terms of critical taper models, northeast Utah and southwest Wyoming. *Geological Society of America Bulletin*, *107*(4), 454. https://doi.org/10.1130/0016-7606(1995)107<0454:HOTSOW>2.3.CO;2

Delph, J. R., Thomas, A. M., & Levander, A. (2021). Subcretionary tectonics: Linking variability in the expression of subduction along the Cascadia forearc. *Earth and Planetary Science Letters*, *556*, 116724. https://doi.org/10.1016/j.epsl.2020.116724

Dickinson, W. R. (1974). *Plate tectonics and sedimentation* (Vol. 22, pp. 1–27). Special Publication SEPM.

Eagles, G. (2016). Plate kinematics of the Rocas Verdes Basin and Patagonian orocline. *Gondwana Research*, *37*, 98–109. https://doi.org/10.1016/j.gr.2016.05.015

Eagles, G., & Scott, B. G. C. (2014). Plate convergence west of Patagonia and the Antarctic Peninsula since 61 Ma. *Global and Planetary Change*, *123*, 189–198. https://doi.org/10.1016/j.gloplacha.2014.08.002

Fanning, C. M., Hervé, F., Pankhurst, R. J., Rapela, C. W., Kleiman, L. E., Yaxley, G. M., & Castillo, P. (2011). Lu-Hf isotope evidence for the provenance of Permian detritus in accretionary complexes of western Patagonia and the northern Antarctic Peninsula region. *Journal of South American Earth Sciences*, *32*(4), 485–496. https://doi.org/10.1016/j.jsames.2011.03.007

Fildani, A., & Hessler, A. M. (2005). Stratigraphic record across a retroarc basin inversion: Rocas Verdes-Magallanes Basin, Patagonian Andes, Chile. *Bulletin of the Geological Society of America*, *117*(11–12), 1596–1614. https://doi.org/10.1130/B25708.1

Flowers, R. M., Farley, K. A., & Ketcham, R. A. (2015). A reporting protocol for thermochronologic modeling illustrated with data from the Grand Canyon. *Earth and Planetary Science Letters*, *432*, 425–435. https://doi.org/10.1016/j.epsl.2015.09.053

Fosdick, J. C., Graham, S. A., & Hilley, G. E. (2014). Influence of attenuated lithosphere and sediment loading on flexure of the deep-water Magallanes retroarc foreland basin, southern Andes. *Tectonics*, *33*(12), 2505–2525. https://doi.org/10.1002/2014TC003684

Fosdick, J. C., Grove, M., Graham, S. A., Hourigan, J. K., Lovera, O., & Romans, B. W. (2015). Detrital thermochronologic record of burial heating and sediment recycling in the Magallanes foreland basin, Patagonian Andes. *Basin Research*, *27*(4), 546–572. https://doi.org/10.1111/bre.12088

Fosdick, J. C., Grove, M., Hourigan, J. K., & Calderón, M. (2013). Retroarc deformation and exhumation near the end of the Andes, southern Patagonia. *Earth and Planetary Science Letters*, *361*, 504–517. https://doi.org/10.1016/j.epsl.2012.12.007

Fosdick, J. C., Romans, B. W., Fildani, A., Bernhardt, A., Calderón, M., & Graham, S. A. (2011). Kinematic evolution of the Patagonian retroarc fold-and-thrust belt and Magallanes foreland basin, Chile and Argentina, 51°30′s. *Bulletin of the Geological Society of America*, *123*(9–10), 1679–1698. https://doi.org/10.1130/B30242.1

Fosdick, J. C., VanderLeest, R. A., Bostelmann, J. E., Leonard, J. S., Ugalde, R., Oyarzún, J. L., & Griffin, M. (2020). Revised timing of Cenozoic Atlantic incursions and changing hinterland sediment sources during southern Patagonian orogenesis. *Lithosphere*, *2020*(1), 1–18. https://doi.org/10.2113/2020/8883099

Furlong, K. P., & Govers, R. (1999). Ephemeral crustal thickening at a triple junction: The Mendocino crustal conveyor. *Geology*, *27*(2), 127–130. https://doi.org/10.1130/0091-7613(1999)027<0127:ECTAAT>2.3.CO;2

Gallardo Jara, R. E., Ghiglione, M. C., Galliani, L. R., & Mpodozis, C. (2022). From rift to foreland basin: A case example from the Magallanes-Austral basin, southernmost Andes. *Basin Research*, 1–33. https://doi.org/10.1111/bre.12739

Garver, J. I. (2003). Etching zircon age standards for fission-track analysis. *Radiation Measurements*, *37*(1), 47–53. https://doi.org/10.1016/S1350-4487(02)00127-0

George, S. W. M., Davis, S. N., Fernández, R. A., Manríquez, L. M. E., Leppe, M. A., Horton, B. K., & Clarke, J. A. (2020). Chronology of deposition and unconformity development across the Cretaceous—Paleogene boundary, Magallanes-Austral Basin, Patagonian Andes. *Journal of South American Earth Sciences*, *97*, 102237. https://doi.org/10.1016/j.jsames.2019.102237

Georgieva, V., Melnick, D., Schildgen, T. F., Ehlers, T. A., Lagabrielle, Y., Enkelmann, E., & Strecker, M. R. (2016). Tectonic control on rock uplift, exhumation, and topography above an oceanic ridge collision: Southern Patagonian Andes (47°S), Chile. *Tectonics*, *35*(6), 1317–1341. https://doi.org/10.1002/2016TC004120

Ghiglione, M. C., & Cristallini, E. O. (2007). Have the southernmost Andes been curved since Late Cretaceous time? An analog test for the Patagonian Orocline. *Geology*, *35*(1), 13–16. https://doi.org/10.1130/G22770A.1

Ghiglione, M. C., Likerman, J., Barberón, V., Beatriz Giambiagi, L., Aguirre-Urreta, B., & Suarez, F. (2014). Geodynamic context for the deposition of coarse-grained deep-water axial channel systems in the Patagonian Andes. *Basin Research*, *26*(6), 726–745. https://doi.org/10.1111/bre.12061

Ghiglione, M. C., Quinteros, J., Yagupsky, D., Bonillo-Martínez, P., Hlebszevtich, J., Ramos, V. A., et al. (2010). Structure and tectonic history of the foreland basins of southernmost South America. *Journal of South American Earth Sciences*, *29*(2), 262–277. https://doi.org/10.1016/j.jsames.2009.07.006

Ghiglione, M. C., & Ramos, V. A. (2005). Progression of deformation and sedimentation in the southernmost Andes. *Tectonophysics*, *405*(1–4), 25–46. https://doi.org/10.1016/j.tecto.2005.05.004

Ghiglione, M. C., Ramos, V. A., & Barberón, V. (2016). Orogenic growth of the Fuegian Andes (52–56°) and their relation to tectonics of the Scotia arc. In A. Folguera (Ed.), *Growth of the southern Andes* (pp. 241–267). Spring International Publishing. https://doi.org/10.1007/978-3-319-23060-3_11

Ghiglione, M. C., Ronda, G., Suárez, R. J., Aramendía, I., Barberón, V., Ramos, M. E., et al. (2019). Structure and tectonic evolution of the South Patagonian fold and thrust belt: Coupling between subduction dynamics, climate and tectonic deformation. *Andean Tectonics*, *28*, 675–697. https://doi.org/10.1016/B978-0-12-816009-1.00024-1

Ghiglione, M. C., Suarez, F., Ambrosio, A., Da Poian, G., Cristallini, E. O., Pizzio, M. F., & Reinoso, R. M. (2009). Structure and evolution of the Austral Basin fold-thrust belt, southern Patagonian Andes. *Revista de la Asociación Geológica Argentina*, *65*(1), 215–226.

Ghiglione, M. C., Yagupsky, D., Ghidella, M., & Ramos, V. A. (2008). Continental stretching preceding the opening of the Drake Passage: Evidence from Tierra del Fuego. *Geology*, *36*(8), 643–646. https://doi.org/10.1130/G24857A.1

Gombosi, D. J., Barbeau, D. L., & Garver, J. I. (2009). New thermochronometric constraints on the rapid Palaeogene exhumation of the Cordillera Darwin complex and related thrust sheets in the Fuegian Andes. *Terra Nova*, *21*(6), 507–515. https://doi.org/10.1111/j.1365-3121.2009.00908.x

Guenthner, W. R., Reiners, P. W., Ketcham, R. A., Nasdala, L., & Giester, G. (2013). Helium diffusion in natural zircon: Radiation damage, anisotropy, and the interpretation of zircon (U-TH)/He thermochronology. *American Journal of Science*, *313*(3), 145–198. https://doi.org/10.2475/03.2013.01

Guillaume, B., Gautheron, C., Simon-Labric, T., Martinod, J., Roddaz, M., & Douville, E. (2013). Dynamic topography control on Patagonian relief evolution as inferred from low temperature thermochronology. *Earth and Planetary Science Letters*, *364*, 157–167. https://doi.org/10.1016/j.epsl.2012.12.036

Guillaume, B., Martinod, J., Husson, L., Roddaz, M., & Riquelme, R. (2009). Neogene uplift of central eastern Patagonia: Dynamic response to active spreading ridge subduction? *Tectonics*, *28*(2), 1–19. https://doi.org/10.1029/2008TC002324

Guillaume, B., Moroni, M., Funiciello, F., Martinod, J., & Faccenna, C. (2010). Mantle flow and dynamic topography associated with slab window opening: Insights from laboratory models. *Tectonophysics*, *496*(1–4), 83–98. https://doi.org/10.1016/j.tecto.2010.10.014

Haschke, M., Sobel, E. R., Blisniuk, P., Strecker, M. R., & Warkus, F. (2006). Continental response to active ridge subduction. *Geophysical Research Letters*, *33*(15), 1–5. https://doi.org/10.1029/2006GL025972

Herman, F., & Brandon, M. (2015). Mid-latitude glacial erosion hotspot related to equatorial shifts in southern Westerlies. *Geology*, *43*(11), 987–990. https://doi.org/10.1130/G37008.1

Herman, F., Seward, D., Valla, P. G., Carter, A., Kohn, B., Willett, S. D., & Ehlers, T. A. (2013). Worldwide acceleration of mountain erosion under a cooling climate. *Nature*, *504*(7480), 423–426. https://doi.org/10.1038/nature12877

Hervé, F., Massonne, H. J., Calderón, M., & Theye, T. (2007). Metamorphic P-T conditions of Late Jurassic rhyolites in the Magallanes fold and thrust belt, Patagonian Andes, Chile. *Journal of Iberian Geology*, *33*(1), 5–16. https://doi.org/10.5209/JIGE.33921

Hervé, F., Pankhurst, R. J., Fanning, C. M., Calderón, M., & Yaxley, G. M. (2007). The South Patagonian batholith: 150 my of granite magmatism on a plate margin. *Lithos*, *97*(3–4), 373–394. https://doi.org/10.1016/j.lithos.2007.01.007

Horton, B. K. (2018). Tectonic regimes of the central and southern Andes: Responses to variations in plate coupling during subduction. *Tectonics*, *37*(2), 402–429. https://doi.org/10.1002/2017TC004624

Horton, B. K. (2022). Unconformity development in retroarc foreland basins: Implications for the geodynamics of Andean-type margins. *Journal of the Geological Society*, *179*(3), jgs2020–263. https://doi.org/10.1144/jgs2020-263

Hubbard, S. M., Romans, B. W., & Graham, S. A. (2008). Deep-water foreland basin deposits of the Cerro Toro Formation, Magallanes basin, Chile: Architectural elements of a sinuous basin axial channel belt. *Sedimentology*, *55*(5), 1333–1359. https://doi.org/10.1111/j.1365-3091.2007.00948.x

Hyppolito, T., Angiboust, S., Juliani, C., Glodny, J., Garcia-Casco, A., Calderón, M., & Chopin, C. (2016). Eclogite-amphibolite- and blueschist-facies rocks from Diego de Almagro Island (Patagonia): Episodic accretion and thermal evolution of the Chilean subduction interface during the Cretaceous. *Lithos*, *264*, 422–440. https://doi.org/10.1016/j.lithos.2016.09.001

Iannelli, S. B., Fernández Paz, L., Litvak, V. D., Gianni, G., Fennell, L. M., González, J., et al. (2020). Southward-directed subduction of the Farallon–Aluk spreading ridge and its impact on subduction mechanics and Andean arc magmatism: Insights from geochemical and seismic tomographic data. *Frontiers of Earth Science*, *8*. https://doi.org/10.3389/feart.2020.00121

Jobe, Z. R., Bernhardt, A., & Lowe, D. R. (2010). Facies and architectural asymmetry in a conglomerate-rich submarine channel fill, Cerro Toro formation, Sierra Del Toro, Magallanes Basin, Chile. *Journal of Sedimentary Research*, *80*(12), 1085–1108. https://doi.org/10.2110/jsr.2010.092

Jordan, T. E. (1995). Retroarc foreland and related basins. *Tectonics of Sedimentary Basins*.

Jordan, T. E., & Allmendinger, R. W. (1986). The Sierras Pampeanas of Argentina; a modern analogue of Rocky Mountain foreland deformation. *American Journal of Science*, *286*(10), 737–764. https://doi.org/10.2475/ajs.286.10.737

Jordan, T. E., Matthew Burns, W., Veiga, R., Pángaro, F., Copeland, P., Kelley, S., & Mpodozis, C. (2001). Extension and basin formation in the southern Andes caused by increased convergence rate: A mid-Cenozoic trigger for the Andes. *Tectonics*, *20*(3), 308–324. https://doi.org/10.1029/1999TC001181

Katz, H. R. (1963). Revision of Cretaceous stratigraphy in Patagonian Cordillera of Ultima Esperanza, Magallanes Province, Chile. *Bulletin of the America Association of Petroleum Geologists*, *47*(3), 506–524.

Kay, S. M., Gorring, M., & Ramos, V. A. (2004). Magmatic sources, setting and causes of Eocene to recent Patagonian plateau magmatism (36°S to 52°S latitude). *Revista de La Asociación Geológica Argentina*, *59*(4), 556–568.

Ketcham, R. A. (2005). Forward and inverse modeling of low-temperature thermochronometry data. *Reviews in Mineralogy and Geochemistry*, *58*(1), 275–314. https://doi.org/10.2138/rmg.2005.58.11

Ketcham, R. A. (2019). Fission-track annealing: From geologic observations to thermal history modeling. In M. G. Malusà, & P. G. Fitzgerald (Eds.), *Fission-track thermochronology and its application to geology* (pp. 49–75). Springer International Publishing. https://doi.org/10.1007/978-3-319-89421-8_3

Klepeis, K. A. (1994). Relationship between uplift of the metamorphic core of the southernmost Andes and shortening in the Magallanes foreland fold and thrust belt, Tierra del Fuego, Chile. *Tectonics*, *13*(4), 882–904. https://doi.org/10.1029/94TC00628

Klepeis, K. A., & Austin, J. A. (1997). Contrasting styles of superposed deformation in the southernmost Andes. *Tectonics*, *16*(5), 755–776. https://doi.org/10.1029/97tc01611

Klepeis, K. A., Betka, P., Clarke, G., Fanning, M., Hervé, F., Rojas, L., et al. (2010). Continental underthrusting and obduction during the Cretaceous closure of the Rocas Verdes rift basin, Cordillera Darwin, Patagonian Andes. *Tectonics*, *29*(3), TC3014. https://doi.org/10.1029/2009TC002610

Kohn, M. J., Spear, F. S., Harrison, T. M., & Dalziel, I. W. D. (1995). $^{40}Ar/^{39}Ar$ geochronology and P-T-t paths from the Cordillera Darwin metamorphic complex, Tierra del Fuego, Chile. *Journal of Metamorphic Geology*, *13*(2), 251–270. https://doi.org/10.1111/j.1525-1314.1995.tb00217.x

Kraemer, P. E. (1998). Structure of the Patagonian Andes: Regional balanced cross section at 50S, Argentina. *International Geology Review*, *40*(10), 896–915. https://doi.org/10.1080/00206819809465244

Kraemer, P. E. (2003). Orogenic shortening and the origin of the Patagonian orocline (56°S.Lat). *Journal of South American Earth Sciences*, *15*(7), 731–748. https://doi.org/10.1016/S0895-9811(02)00132-3

Lagabrielle, Y., Goddéris, Y., Donnadieu, Y., Malavieille, J., & Suarez, M. (2009). The tectonic history of Drake Passage and its possible impacts on global climate. *Earth and Planetary Science Letters*, *279*(3–4), 197–211. https://doi.org/10.1016/j.epsl.2008.12.037

Maffione, M., Speranza, F., Faccenna, C., & Rossello, E. (2010). Paleomagnetic evidence for a pre-early Eocene (~50 Ma) bending of the Patagonian orocline (Tierra del Fuego, Argentina): Paleogeographic and tectonic implications. *Earth and Planetary Science Letters*, *289*(1–2), 273–286. https://doi.org/10.1016/j.epsl.2009.11.015

Malkowski, M. A., Grove, M., & Graham, S. A. (2016). Unzipping the Patagonian Andes—Long-lived influence of rifting history on foreland basin evolution. *Lithosphere*, *8*(1), 23–28. https://doi.org/10.1130/L489.1

Maloney, K. T., Clarke, G. L., Klepeis, K. A., & Quevedo, L. (2013). The Late Jurassic to present evolution of the Andean margin: Drivers and the geological record. *Tectonics*, *32*(5), 1049–1065. https://doi.org/10.1002/tect.20067

Malumián, N., & Olivero, E. B. (1998). La Formación Río Bueno, relaciones estratigráficas y edad, Eoceno inferior, Isla Grande de Tierra del Fuego, Argentina. In *X Congreso Latinoamericano de Geología* (pp. 120–124).

Malumián, N., Panza, J. L., Parisi, C., Nañez, C., Caramés, A., & Torre, A. (2000). Hoja Geológica 5172-III, Yacimiento Río Tur-bio (1:250,000). *Servicio Geológico Minero Argentino, Boletin*, *247*, 180.

McAtamney, J., Klepeis, K., Mehrtens, C., Thomson, S., Betka, P., Rojas, L., & Snyder, S. (2011). Along-strike variability of back-arc basin collapse and the initiation of sedimentation in the Magallanes foreland basin, southernmost Andes (53-54.5S). *Tectonics*, *30*(5), 1–26. https://doi.org/10.1029/2010TC002826

Metcalf, J. R., Fitzgerald, P. G., Baldwin, S. L., & Muñoz, J. A. (2009). Thermochronology of a convergent orogen: Constraints on the timing of thrust faulting and subsequent exhumation of the Maladeta Pluton in the Central Pyrenean Axial Zone. *Earth and Planetary Science Letters*, *287*(3–4), 488–503. https://doi.org/10.1016/j.epsl.2009.08.036

Muller, V. A. P., Calderón, M., Fosdick, J. C., Ghiglione, M. C., Cury, L. F., Massonne, H.-J., et al. (2021). The closure of the Rocas Verdes Basin and early tectono-metamorphic evolution of the Magallanes fold-and-thrust belt, southern Patagonian Andes (52–54°S). *Tectonophysics*, *798*, 228686. https://doi.org/10.1016/j.tecto.2020.228686

Murray, K. E., Goddard, A. L. S., Abbey, A. L., & Wildman, M. (2022). Thermal history modeling techniques and interpretation strategies: Applications using HeFTy. *Geosphere*, *18*(X), 1–21. https://doi.org/10.1130/GES02500.1/5677788/ges02500.pdf

Navarrete, C., Gianni, G., Massaferro, G., & Butler, K. (2020). The fate of the Farallon slab beneath Patagonia and its links to Cenozoic intraplate magmatism, marine transgressions and topographic uplift. *Earth-Science Reviews*, *210*, 103379. https://doi.org/10.1016/j.earscirev.2020.103379

Nelson, E. P. (1982). Post-tectonic uplift of the Cordillera Darwin orogenic core complex: Evidence from fission track geochronology and closing temperature—Time relationships. *Journal of the Geological Society*, *139*(6), 755–761. https://doi.org/10.1144/gsjgs.139.6.0755

Olivero, E. B., Malumián, N., Palamarczuk, S., & Scasso, R. A. (2001). El Cretácico superior-Paleogeno del área del Río Bueno, costa. *Revista de La Asociación Geológica Argentina*, *57*(3), 199–218.

Pankhurst, R. J., Rapela, C. W., & Fanning, C. M. (2000). Age and origin of coeval TTG, I- and S-type granites in the Famatinian belt of NW Argentina. *Earth and Environmental Science Transactions of the Royal Society of Edinburgh*, *91*(1–2), 151–168. https://doi.org/10.1017/s0263593300007343

Pevear, D. R. (1992). Illite age analysis: A new tool for basin thermal history analysis. In Y. M. Kharaka, & A. Maest (Eds.), *Water-rock interaction: Proceedings of the 7th international symposium* (pp. 1251–1254).

Poblete, F., Roperch, P., Hervé, F., Diraison, M., Espinoza, M., & Arriagada, C. (2014). The curved Magallanes fold and thrust belt: Tectonic insights from a paleomagnetic and anisotropy of magnetic susceptibility study. *Tectonics*, *33*(12), 2526–2551. https://doi.org/10.1002/2014TC003555

Ramírez de Arellano, C., Calderón, M., Rivera, H., Valenzuela, M., Fanning, C. M., & Paredes, E. (2021). Neogene Patagonian magmatism between the rupture of the Farallon plate and the Chile Ridge subduction. *Journal of South American Earth Sciences*, *110*, 103238. https://doi.org/10.1016/j.jsames.2021.103238

Ramos, V. A. (2005). Seismic ridge subduction and topography: Foreland deformation in the Patagonian Andes. *Tectonophysics*, *399*(1–4), 73–86. https://doi.org/10.1016/j.tecto.2004.12.016

Ramos, V. A. (1989). Andean foothills structures in northern Magallanes basin, Argentina. *American Association of Petroleum Geologists Bulletin*, *73*(7), 887–903. https://doi.org/10.1306/44B4A28A-170A-11D7-8645000102C1865D

Ramos, V. A., & Folguera, A. (2009). Andean flat-slab subduction through time. *Geological Society, London, Special Publications*, *327*(1), 31–54. https://doi.org/10.1144/SP327.3

Ramos, V. A., & Ghiglione, M. C. (2008). The Late Cenozoic of Patagonia and Tierra del Fuego. *Developments in Quaternary Science*, *11*, 57–71. https://doi.org/10.1016/S1571-0866(07)10004-X

Reiners, P. W., Spell, T. L., Nicolescu, S., & Zanetti, K. A. (2004). Zircon (U-Th)/He thermochronometry: He diffusion and comparisons with $^{40}Ar/^{39}Ar$ dating. *Geochimica et Cosmochimica Acta*, *68*(8), 1857–1887. https://doi.org/10.1016/j.gca.2003.10.021

Romans, B. W., Fildani, A., Graham, S. A., Hubbard, S. M., & Covault, J. A. (2010). Importance of predecessor basin history on sedimentary fill of a retroarc foreland basin: Provenance analysis of the Cretaceous Magallanes basin, Chile (50-52°S). *Basin Research*, *22*(5), 640–658. https://doi.org/10.1111/j.1365-2117.2009.00443.x

Romans, B. W., Fildani, A., Hubbard, S. M., Covault, J. A., Fosdick, J. C., & Graham, S. A. (2011). Evolution of deep-water stratigraphic architecture, Magallanes Basin, Chile. *Marine and Petroleum Geology*, *28*(3), 612–628. https://doi.org/10.1016/j.marpetgeo.2010.05.002

Ronda, G., Ghiglione, M., Martinod, J., Barberón, V., Ramos, M. E., Coutand, I., et al. (2022). Early Cretaceous to Cenozoic growth of the Patagonian Andes as revealed by low-temperature thermochronology. *Tectonics*, *41*(10), 1–23. https://doi.org/10.1029/2021tc007113

Scher, H. D., & Martin, E. E. (2006). Timing and climatic consequences of the opening of Drake Passage. *Science*, *312*(5772), 428–430. https://doi.org/10.1126/science.1120044

Schwartz, T. M., Fosdick, J. C., & Graham, S. A. (2017). Using detrital zircon U-Pb ages to calculate Late Cretaceous sedimentation rates in the Magallanes-Austral basin, Patagonia. *Basin Research*, *29*(6), 725–746. https://doi.org/10.1111/bre.12198

Schwartz, T. M., & Graham, S. A. (2015). Stratigraphic architecture of a tide-influenced shelf-edge delta, Upper Cretaceous Dorotea Formation, Magallanes-Austral Basin, Patagonia. *Sedimentology*, *62*(4), 1039–1077. https://doi.org/10.1111/sed.12176

Scott, K. M. (1966). Sedimentology and dispersal pattern of a Cretaceous flysch sequence, Patagonian Andes, southern Chile. *Bulletin of the America Association of Petroleum Geologists*, *50*(1), 72–107.

SERNAGEOMIN. (2003). *Mapa Geológico de Chile: Version digital. publicación geológica digital, No. 4, 2003. CDROM, versión 1.0, 2003. Base Geológica escala 1:1.000.000. Gobierno de Chile*. Servicio Nacional de Geología y Minería, Subdirección Nacional de Geología.

Sickmann, Z. T., Schwartz, T. M., & Graham, S. A. (2018). Refining stratigraphy and tectonic history using detrital zircon maximum depositional age: An example from the Cerro Fortaleza formation, Austral Basin, southern Patagonia. *Basin Research*, *30*(4), 708–729. https://doi.org/10.1111/bre.12272

Somoza, R., & Ghidella, M. E. (2012). Late Cretaceous to recent plate motions in western South America revisited. *Earth and Planetary Science Letters*, *331*(332), 152–163. https://doi.org/10.1016/j.epsl.2012.03.003

Środoń, J., Clauer, N., & Eberl, D. D. (2002). Interpretation of K-Ar dates of illitic clays from sedimentary rocks aided by modeling. *American Mineralogist*, *87*(11–12), 1528–1535. https://doi.org/10.2138/am-2002-11-1202

Stern, C. R., & de Wit, M. J. (2004). *Rocas Verdes ophiolites, southernmost South America: Remnants of progressive stages of development of oceanic-type crust in a continental margin back-arc basin* (Vol. 218, pp. 665–683). Geological Society Special Publication. https://doi.org/10.1144/GSL.SP.2003.218.01.32

Stevens Goddard, A. L., & Fosdick, J. C. (2019). Multichronometer thermochronologic modeling of migrating spreading ridge subduction in southern Patagonia. *Geology*, *47*(6), 555–558. https://doi.org/10.1130/g46091.1

Süssenberger, A., Schmidt, S. T., Wemmer, K., Baumgartner, L. P., & Grobéty, B. (2018). Timing and thermal evolution of fold-and-thrust belt formation in the Ultima Esperanza District, 51°S Chile: Constraints from K-Ar dating and illite characterization. *Geological Society of America Bulletin*, *130*(5–6), 1–24. https://doi.org/10.1130/B31766.1

ter Voorde, M., de Bruijne, C. H., Cloetingh, S. A. P. L., & Andriessen, P. A. M. (2004). Thermal consequences of thrust faulting: Simultaneous versus successive fault activation and exhumation. *Earth and Planetary Science Letters*, *223*(3–4), 395–413. https://doi.org/10.1016/j.epsl.2004.04.026

Thomson, S. N., Brandon, M. T., Tomkin, J. H., Reiners, P. W., Vásquez, C., & Wilson, N. J. (2010). Glaciation as a destructive and constructive control on mountain building. *Nature*, *467*(7313), 313–317. https://doi.org/10.1038/nature09365

Thomson, S. N., Hervé, F., & Stöckhert, B. (2001). Mesozoic-Cenozoic denudation history of the Patagonian Andes (southern Chile) and its correlation to different subduction processes. *Tectonics*, *20*(5), 693–711. https://doi.org/10.1029/2001tc900013

Thorkelson, D. J. (1996). Subduction of diverging plates and the principles of slab window formation. *Tectonophysics*, *255*(1–2), 47–63. https://doi.org/10.1016/0040-1951(95)00106-9

Torres Carbonell, P. J., Cao, S. J., González Guillot, M., Mosqueira González, V., Dimieri, L. V., Duval, F., & Scaillet, S. (2020). The Fuegian thrust-fold belt: From arc-continent collision to thrust-related deformation in the southernmost Andes. *Journal of South American Earth Sciences*, *102*, 102678. https://doi.org/10.1016/j.jsames.2020.102678

Torres Carbonell, P. J., & Olivero, E. B. (2019). Tectonic control on the evolution of depositional systems in a fossil, marine foreland basin: Example from the SE Austral Basin, Tierra del Fuego, Argentina. *Marine and Petroleum Geology*, *104*, 40–60. https://doi.org/10.1016/j.marpetgeo.2019.03.022

Torres Carbonell, P. J., Olivero, E. B., & Dimieri, L. V. (2008). Structure and evolution of the Fuegian Andes foreland thrust-fold belt, Tierra del Fuego, Argentina: Paleogeographic implications. *Journal of South American Earth Sciences*, *25*(4), 417–439. https://doi.org/10.1016/j.jsames.2007.12.002

Torres García, M. F., Calderón, M., Ramírez de Arellano, C., Hervé, F., Opitz, J., Theye, T., et al. (2020). Trace element composition of amphibole and petrogenesis of hornblendites and plutonic suites of Cretaceous magmatic arcs developed in the Fuegian Andes, southernmost South America. *Lithos*, *372–373*, 105656. https://doi.org/10.1016/j.lithos.2020.105656

van de Lagemaat, S. H. A., Swart, M. L. A., Vaes, B., Kosters, M. E., Boschman, L. M., Burton-Johnson, A., et al. (2021). Subduction initiation in the Scotia Sea region and opening of the Drake Passage: When and why? *Earth-Science Reviews*, *215*, 103551. https://doi.org/10.1016/j.earscirev.2021.103551

VanderLeest, R. A., Fosdick, J. C., Leonard, J. S., & Morgan, L. (2020). Early Miocene volcanism between slab windows revealed from detrital $^{40}Ar/^{39}Ar$ geochronology and geochemistry of the Magallanes Basin 50-52°S. *Journal of Geodynamics*, *125*, 101751. https://doi.org/10.1016/j.jog.2020.101751

VanderLeest, R. A., Fosdick, J. C., Malkowski, M. A., Romans, B. W., Ghiglione, M. C., Schwartz, T. M., & Sickmann, Z. T. (2022). Tectonic subsidence modeling of diachronous transition from backarc to retroarc basin development and uplift during Cordilleran orogenesis, Patagonian-Fuegian Andes. *Tectonics*, *41*(10), 1–29. https://doi.org/10.1029/2021tc006891

Willett, C. D., Ma, K. F., Brandon, M. T., Hourigan, J. K., Christeleit, E. C., & Shuster, D. L. (2020). Transient glacial incision in the Patagonian Andes from ∼6 Ma to present. *Science Advances*, *6*(7), 1–10. https://doi.org/10.1126/sciadv.aay1641

Willner, A. P., Hervé, F., Thomson, S. N., & Massonne, H. J. (2004). Converging P-T paths of Mesozoic HP-LT metamorphic units (Diego de Almagro Island, Southern Chile): Evidence for juxtaposition during late shortening of an active continental margin. *Mineralogy and Petrology*, *81*(1–2), 43–84. https://doi.org/10.1007/s00710-004-0033-9

Willner, A. P., Sepúlveda, F. A., Hervé, F., Massonne, H. J., & Sudo, M. (2009). Conditions and timing of pumpellyite-actinolite-facies metamorphism in the early Mesozoic frontal accretionary prism of the Madre de Dios archipelago (Latitude 50°20′S; Southern Chile). *Journal of Petrology*, *50*(11), 2127–2155. https://doi.org/10.1093/petrology/egp071

Wilson, T. J. (1991). Transition from back-arc to foreland basin development in the southernmost Andes: Stratigraphic record from the Ultima Esperanza District, Chile. *Geological Society of America Bulletin*, *103*(1), 98–111. https://doi.org/10.1130/0016-7606(1991)103<0098:TFBATF>2.3.CO;2

Winn, R. D., & Dott, R. H. (1979). Deep-water fan-channel conglomerates of Late Cretaceous age, southern Chile. *Sedimentology*, *26*(2), 203–228. https://doi.org/10.1111/j.1365-3091.1979.tb00351.x

Wolf, R. A., Farley, K. A., & Kass, D. M. (1998). Modeling of the temperature sensitivity of the apatite (U-Th)/He thermochronometer. *Chemical Geology*, *148*(1–2), 105–114. https://doi.org/10.1016/S0009-2541(98)00024-2

Xie, X., & Heller, P. L. (2009). Plate tectonics and basin subsidence history. *Bulletin of the Geological Society of America*, *121*(1–2), 55–64. https://doi.org/10.1130/B26398.1

Yonkee, W. A., & Weil, A. B. (2015). Tectonic evolution of the Sevier and Laramide belts within the North American Cordillera orogenic system. *Earth-Science Reviews*, *150*, 531–593. https://doi.org/10.1016/j.earscirev.2015.08.001

Zaun, P. E., & Wagner, G. A. (1985). Fission-track stability in zircons under geological conditions. *Nuclear Tracks and Radiation Measurements (1982)*, *10*(3), 303–307. https://doi.org/10.1016/0735-245X(85)90119-X

## References From the Supporting Information


Ault, A. K., Flowers, R. M., & Bowring, S. A. (2013). Phanerozoic surface history of the Slave craton. *Tectonics*, *32*(5), 1066–1083. https://doi.org/10.1002/tect.20069

Flowers, R. M., Bowring, S. A., & Reiners, P. W. (2006). Low long-term erosion rates and extreme continental stability documented by ancient (U-Th)/He dates. *Geology*, *34*(11), 925–928. https://doi.org/10.1130/G22670A.1

Flowers, R. M., Ketcham, R. A., Enkelmann, E., Gautheron, C., Reiners, P. W., Metcalf, J. R., et al. (2022). (U-Th)/He chronology: Part 2. Considerations for evaluating, integrating, and interpreting conventional individual aliquot data, 1–25. https://doi.org/10.1130/B36268.1/5590020/b36268.pdf

Georgieva, V., Gallagher, K., Sobczyk, A., Sobel, E. R., Schildgen, T. F., Ehlers, T. A., & Strecker, M. R. (2019). Effects of slab-window, alkaline volcanism, and glaciation on thermochronometer cooling histories, Patagonian Andes. *Earth and Planetary Science Letters*, *511*, 164–176. https://doi.org/10.1016/j.epsl.2019.01.030

Gleadow, A. J. W., Kohn, B. P., Brown, R. W., O'Sullivan, P. B., & Raza, A. (2002). Fission track thermotectonic imaging of the Australian continent. *Tectonophysics*, *349*(1–4), 5–21. https://doi.org/10.1016/S0040-1951(02)00043-4

Ketcham, R. A., Gautheron, C., & Tassan-Got, L. (2011). Accounting for long alpha-particle stopping distances in (U-Th-Sm)/He geochronology: Refinement of the baseline case. *Geochimica et Cosmochimica Acta*, *75*(24), 7779–7791. https://doi.org/10.1016/j.gca.2011.10.011

Kohn, B., & Gleadow, A. (2019). *Application of low-temperature thermochronology to Craton evolution*. Springer International Publishing. https://doi.org/10.1007/978-3-319-89421-8_21

Ortiz, G., Stevens Goddard, A. L., Fosdick, J. C., Alvarado, P., Carrapa, B., & Cristofolini, E. (2021). Fault reactivation in the Sierras Pampeanas resolved across Andean extensional and compressional regimes using thermochronologic modeling. *Journal of South American Earth Sciences*, *112*(P1), 103533. https://doi.org/10.1016/j.jsames.2021.103533

Rapalini, A. E., Calderón, M., Singer, S., Hervé, F., & Cordani, U. (2008). Tectonic implications of a paleomagnetic study of the Sarmiento Ophiolitic Complex, southern Chile. *Tectonophysics*, *452*(1–4), 29–41. https://doi.org/10.1016/j.tecto.2008.01.005

Reiners, P. W., & Brandon, M. T. (2006). Using thermochronology to understand orogenic erosion. *Annual Review of Earth and Planetary Sciences*, *34*(1), 419–466. https://doi.org/10.1146/annurev.earth.34.031405.125202

Ring, U., Brandon, M. T., Willett, S. D., & Lister, G. S. (1999). *Exhumation processes* (Vol. 154, pp. 1–27). Geological Society, London, Special Publications.

Wildman, M., Brown, R., Persano, C., Beucher, R., Stuart, F. M., Mackintosh, V., et al. (2017). Contrasting Mesozoic evolution across the boundary between on and off craton regions of the South African plateau inferred from apatite fission track and (U-Th-Sm)/He thermochronology. *Journal of Geophysical Research: Solid Earth*, *122*(2), 1517–1547. https://doi.org/10.1002/2016JB013478

Wilson, T. J. (1983). *Stratigraphic and structural evolution of the Ultima Esperanza foreland fold-thrust belt, Patagonian Andes, southern Chile*. Columbia University.